

Identifying and Characterizing Very Low Mass Spectral Blend Binaries with Machine Learning Methods

JUAN DIEGO DRAXL GIANNONI,^{1,2} MALINA DESAI,³ ADAM J. BURGASSER,⁴
A. CAMILLE DUNNING,⁵ CHRISTIAN AGANZE,⁶ LUKE MCDERMOTT,⁷
CHRISTOPHER A. THEISSEN,⁸ AND DANIELLA C. BARDALEZ GAGLIUFFI⁹

¹*Department of Physics, UC San Diego, La Jolla, CA, USA*

²*Department of Aerospace and Geodesy TUM School of Engineering and Design, Technische Universität München, München, Germany*

³*Department of Physics, MIT, Cambridge, MA, USA*

⁴*Department of Astronomy & Astrophysics, UC San Diego, La Jolla, CA 92093, USA*

⁵*Halıcioğlu Data Science Institute, UC San Diego, La Jolla, CA, USA*

⁶*Kavli Institute for Particle Astrophysics & Cosmology, Stanford University, Stanford, CA 94305, USA*

⁷*Department of Computer Science and Engineering, UC San Diego, La Jolla, CA, USA*

⁸*Department of Astronomy & Astrophysics, UC San Diego, La Jolla, CA, USA*

⁹*Department of Physics & Astronomy, Amherst College, Amherst, MA, USA*

(Received TBD; Revised #2 December 16, 2025; Accepted TBD)

Submitted to ApJ

ABSTRACT

We present an approach to identifying and characterizing unresolved, very low mass spectral blend binaries composed of late-M, L, and T dwarfs using machine learning methodologies. We generated and evaluated a series of hierarchical random forest models to distinguish spectral blends from single very low-mass dwarfs, and to classify their primary and secondary components. Models were trained on a sample of single and synthesized binary templates generated from empirical spectra. We explored various aspects of the design of our models, and find that models trained on a full range of single and binary combinations have the best performance for identification and component classification. These models achieve binary identification recall and precision of $\gtrsim 85\%$, median component classification errors of $\lesssim 0.1$ subtypes, and systematic classification uncertainties of $\lesssim 1$ subtype, outperforming index-based methods in terms of fidelity, range, and speed. Optimal performance is achieved for binaries composed of L and T dwarf primaries and late-L and T dwarf secondaries. When applied to the spectra of previously confirmed very low-mass binaries, model performance is degraded due to the prevalence of systems with similar component types, but remains high in the optimal performance range. We propose potential improvements to these models, which can be used to explore binary populations among

the thousands to millions of very low-mass stars and brown dwarfs anticipated with large-scale spectral surveys such as SPHEREx and Euclid.

Keywords: Binary stars (154) — Brown dwarfs (185) — L dwarfs (894) — M dwarfs (982) — T dwarfs (1679) — Random forests (1935)

1. INTRODUCTION

Binary systems containing very low mass (VLM; $M \leq 0.1 M_{\odot}$) stars and brown dwarfs are important benchmarks for testing theories of star and brown dwarf formation and evolution, measuring fundamental parameters such as mass and radius, and calibrating empirical relations connecting observables to physical properties. The majority of VLM binaries known today are resolved systems identified and measured through high angular resolution imaging methods (Fontanive et al. 2018), and have angular separations $\rho \gtrsim 0''.1$, implying orbital semi-major axes $a \gtrsim 1$ au and periods $P \gtrsim 3$ yr at distances of 10 pc or larger (Burgasser et al. 2007b; Bardalez Gagliuffi et al. 2015). While over two dozen of these systems have partial or complete orbit determinations (e.g., Konopacky et al. 2010; Dupuy & Liu 2017), an unknown number of systems with shorter orbit periods remain undetected due to imaging resolution limits. Other techniques to identify unresolved binaries, such as high-resolution spectroscopic monitoring (e.g., Basri & Martín 1999; Blake et al. 2007; Hsu et al. 2021), astrometric monitoring (e.g., Sahlmann et al. 2020), and the detection of overluminous sources (e.g., Manjavacas et al. 2013; Kirkpatrick et al. 2019) have uncovered several VLM binaries with smaller separations, including three eclipsing systems that provide radius measurements (Stassun et al. 2006; Lodieu et al. 2015; Triaud et al. 2020). These methods are resource-intensive, however, with low yields ($\lesssim 1\text{--}10\%$; Jørgens 2008; Sahlmann et al. 2014) and often incomplete determination of orbital and component parameters.

The distinct spectral characteristics of the late-type M, L, T, and Y dwarfs that comprise the very low mass regime enable an alternative method for identifying unresolved binaries as spectral blend binaries. This method, also used in the detection of unresolved M dwarf plus white dwarf pairs (e.g., Raymond et al. 2003; Rebassa-Mansergas et al. 2010; Morgan et al. 2012), is applicable in the VLM regime due to the emergence of distinct molecular features in each spectral class. In particular, the conversion of CO to CH₄ in the T dwarfs ($T_{eff} \lesssim 1400$ K) produces distinct spectral features in blended light spectra even when components differ in brightness by several magnitudes. The prototypical VLM spectral blend binary is 2MASS J0518–2828AB, an L6 plus T4 system initially identified as a peculiar L dwarf, whose near-infrared spectrum could be explained as a blended light source (Cruz et al. 2004a). This system was subsequently confirmed to be a binary by resolved Hubble Space Telescope imaging observations (Burgasser et al. 2006c). To date, over 60 VLM spectral blend

binary candidates and confirmed binary systems have been identified (e.g., [Burgasser et al. 2010a](#); [Bardalez Gagliuffi et al. 2014](#); [Best et al. 2015](#); [Bravo et al. 2023](#)), including sources with measured orbital periods <1 yr (e.g., [Blake et al. 2008](#); [Burgasser et al. 2012b](#); [Sahlmann et al. 2020](#)).

[Burgasser et al. \(2010a, hereafter B10\)](#) and [Bardalez Gagliuffi et al. \(2014, hereafter B14\)](#) developed spectral index-based methods for identifying very low mass spectral blend binaries. Both approaches rely on the contaminating signatures of CH_4 absorption in a combined-light spectrum from a T dwarf companion. While these approaches have uncovered dozens of candidate and confirmed VLM binaries, they are based on an ad-hoc choice of indices and selection criteria that can result in contamination from non-binary sources such as variable brown dwarfs (e.g. [Radigan et al. 2014](#); [Ashraf et al. 2022](#)) and unusually blue L dwarfs (B14), and insensitivity to VLM pairs with equivalent spectral classification or extreme brightness ratios. These biases, and the degeneracies between age, mass, and spectral appearance for cooling brown dwarfs, make it difficult to infer the underlying VLM binary fraction from samples of spectral blend systems ([Bardalez Gagliuffi 2017](#)).

Recently, supervised and unsupervised machine learning (ML) algorithms have been deployed to problems of astrophysical source identification and classification ([Baron 2019](#)). These algorithms can efficiently discern patterns in complex datasets, providing insight into underlying parameters or identifying clusters of sources with common traits. One popular ML approach is the supervised learning method of random forests (RF), which uses an ensemble of uncorrelated decision trees to classify or infer trends in complex data ([Breiman 2001](#)). Each decision tree splits a dataset (features) through a series of threshold values (branches), which are iteratively updated and pruned by training on pre-classified (labeled) data. The results of the decision trees can be aggregated by averaging (regression) or majority voting (classification). RF models have been used extensively for the analysis of spectral data, to classify white dwarfs ([García-Zamora et al. 2023](#)) and VLM dwarfs ([Feaser & Best 2022](#); [Zhou et al. 2024](#)), and to infer the physical properties of galaxies ([Anghopo et al. 2024](#)), A-type stars ([Chen et al. 2022](#)), and VLM dwarfs ([Lueber et al. 2022](#)), among other applications. Relevant to this work, [Aganze et al. \(2022\)](#) demonstrated that ML algorithms are superior to index-based methods in identifying and classifying VLM dwarfs in large spectroscopic surveys, significantly reducing contamination, an important consideration when the sources of interest comprise a small fraction ($<1\%$) of the overall sample.

Recognizing the benefits of machine learning methods to spectral classification problems, we examined the application of the random forest algorithm to the identification and characterization of very low mass spectral blend binaries. This work follows a pilot study by [Desai et al. \(2023\)](#) which demonstrated 95% precision in identifying spectral blends of M7–L7 plus T1–T8 pairs. Here we expand this analysis to cover a broader set of binary combinations, and explore further details in the construction and

training of the RF models. This article is organized as follows: Section 2 describes the input spectral sample and training set for our models, and benchmarks our analysis by quantifying the precision and accuracy of the B10 and B14 index-based methods. Section 3 describes the design and training of the RF models used for binary identification and component classification. Section 4 reviews performance of the models for various assumptions of input training data, data quality, and component composition. Section 5 further validates the performance of these models against a sample of confirmed binary spectra. Section 6 discusses limitations to this study in terms of sample and model design, selection biases, and the typical compositions of VLM binaries in volume-limited samples. Finally, Section 7 summarizes our findings and prospects for VLM binary searches in future spectral surveys.

2. MODEL TRAINING DATA

2.1. Spectral Sample

Our training sample was constructed from low-resolution, near-infrared spectra of late-M, L and T dwarfs contained in the SpeX Prism Library Analysis Toolkit (SPLAT; Burgasser & Splat Development Team 2017), obtained with the SpeX spectrograph on the NASA 3m Infrared Telescope Facility (Rayner et al. 2003). We started with approximately 1500 VLM dwarf spectra with published spectral types spanning M6 to T9. This initial sample was curated by removing previously reported binaries and spectral binary candidates, young brown dwarfs, subdwarfs, and misclassified giant stars. For sources with multiple spectral observations, we selected the spectrum with the highest signal-to-noise (S/N). We also conducted a visual inspection to remove other contaminants, and removed any spectra with undefined, infinite, or negative values in their flux or uncertainty arrays to ensure accurate S/N calculations. All spectra were interpolated onto a common wavelength scale spanning 0.9–2.4 μm , aligned with the pixel scale for a representative spectrum with an average resolution of $\lambda/\Delta\lambda \approx 100$. Spectra were reclassified by direct comparison to near-infrared standards defined in Kirkpatrick et al. (2010, M and L dwarfs) and Burgasser et al. (2006b, T dwarfs). The final template sample of 1006 spectra is summarized in the Appendix.

2.2. Synthetic Single Templates

Figure 1 displays the distributions of spectral types and signal-to-noise ratios for these template spectra, the latter calculated in the 1.20–1.35 μm *J*-band flux peak to accommodate the strong absorption features present in late-L and T dwarf spectra. The distribution of spectral types is highly asymmetric due to the intrinsic brightnesses of the sources and the underlying luminosity function, both of which vary considerably with spectral type (Bardalez Gagliuffi et al. 2019a; Kirkpatrick et al. 2024). Our initial exploration of RF models indicated that such unbalanced samples can lead to significant biases in classification (Desai et al. 2023). In addition, vary-

ing S/N is of particular concern as the subtle absorption features from a companion spectrum can be obscured by noise in a low S/N spectrum.

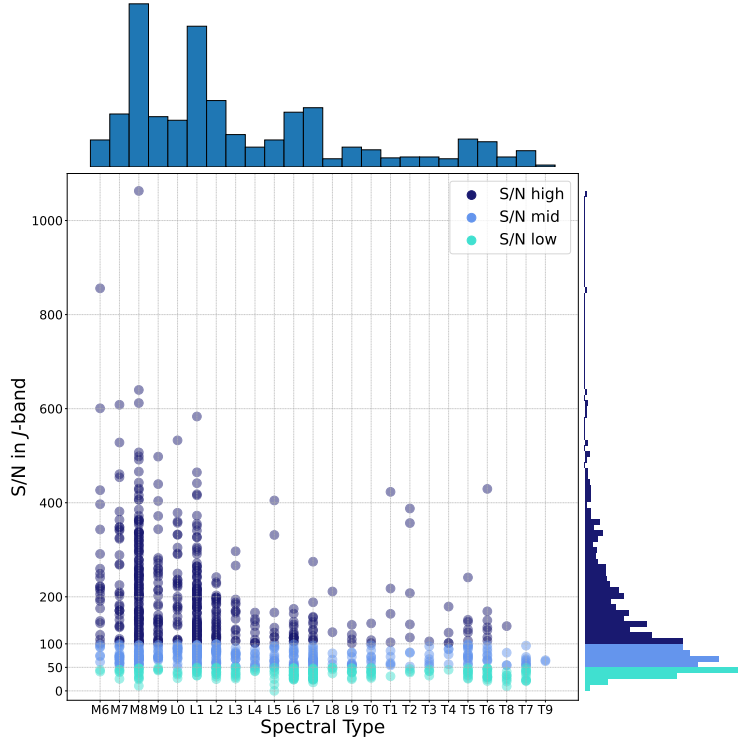


Figure 1. *J*-band signal-to-noise (S/N) vs spectral type of our empirical spectral sample. Each individual spectrum is plotted and color-coded by their assignment to low ($S/N < 50$, light blue), mid ($50 \leq S/N < 100$, medium blue), and high ($S/N \geq 100$, dark blue) S/N groups. We show the marginalized distributions of the spectral type along the top axis, and for S/N along the right axis.

To address these sample imbalances, we constructed a synthetic dataset of single templates evenly-distributed across spectral types M6 to T9 and across signal-to-noise ratios through noise scaling and flux resampling. We defined three *J*-band S/N groups: low ($2 \leq S/N < 50$), mid ($50 \leq S/N < 100$), and high ($S/N \geq 100$), and developed separate RF models for each of these groups. For each spectral subtype, we first chose a subsample of SpeX spectra with *J*-band S/N equal to or greater than our target S/N range. We randomly selected spectra from this subsample with replacement, then varied the spectral fluxes using Monte Carlo methods, drawing a new flux value at each wavelength from a Gaussian distribution centered on the original flux value and with a width equal to the uncertainty. We generated lower S/N spectra in this process by scaling up the uncertainty before resampling. We re-computed the *J*-band S/N and the standard-match classification for each new synthetic spectrum. This process was repeated across all spectral subtypes until we had created a sample of 17,060 synthetic templates, distributed as 250 templates per subtype for 24 subtypes spanning M6 to T9 for the low and mid S/N groups (6,000 templates each); and 230 templates per subtype for 22 subtypes spanning M6 to T9

for the high S/N group, excluding T7 and T9 which lacked high S/N SpeX spectra (5,060 templates).

2.3. *Synthetic Binary Templates*

We created an evenly-distributed sample of synthetic binary templates following a similar approach as our single templates, accounting for equal representation of primary and secondary spectral type combinations as well as signal-to-noise groupings. We first scaled all of the SpeX spectra to absolute fluxes using the Dupuy & Liu (2012) absolute magnitude/spectral type relation for the 2MASS J -band filter. This relation has an inherent uncertainty of 0.4 mag. Our baseline analysis does not account for this uncertainty; however, we evaluated its influence in one set of binary identification models as discussed in Section 3.1. We selected subsamples of spectra matching the intended primary and secondary subtypes (secondaries were required to have the same or later classifications), and with S/N values equal to or greater than our intended binary template S/N. We randomly paired primary and secondary templates from these subsamples, added the spectral fluxes (uncertainties were combined in quadrature), and re-normalized the combined template between 1.20–1.35 μm to mitigate selection biases (Desai et al. 2023). We expanded the number of spectra within each primary-secondary classification and S/N groupings using the same Monte Carlo approach as our single templates. The resulting binary templates were then re-classified by comparison to spectral standards and the J -band S/N re-computed. An example of a synthetic binary template for an L5 plus T5 combination in the mid S/N group is illustrated in Figure 2. This process was repeated to generate 20 binaries for each of the 300 primary-secondary combinations, yielding 6,000 synthetic binary templates for each of the low and mid S/N groups. For the high S/N group, the absence of high S/N T7 and T9 spectra reduced the number of possible pairings to 253, yielding 5,060 binary templates. The size of the synthetic binary template sample intentionally matches the size of the synthetic single template sample for each S/N group.

2.4. *Benchmarking Spectral Index Methods*

In order to assess the utility of our machine learning approach, we quantified the performance of the original index-based selection methods of B10 and B14 using our template sample. For L dwarf plus T dwarf binaries, B10 used eight spectral indices and near-infrared spectral types to establish six selection criteria that segregate spectral binaries from single stars. Objects satisfying at least three criteria were considered “strong” binary candidates, those satisfying only two criteria were considered “weak” candidates, based on the sources known to be binary at the time of the study. B10 also compared the χ^2 deviation between a candidate spectrum ($S[\lambda]$) and both best-fit single and binary templates ($T[\lambda]$),

$$\chi^2 \equiv \sum_{\lambda} \left[\frac{S[\lambda] - \alpha T[\lambda]}{\sigma_S[\lambda]} \right]^2 \quad (1)$$

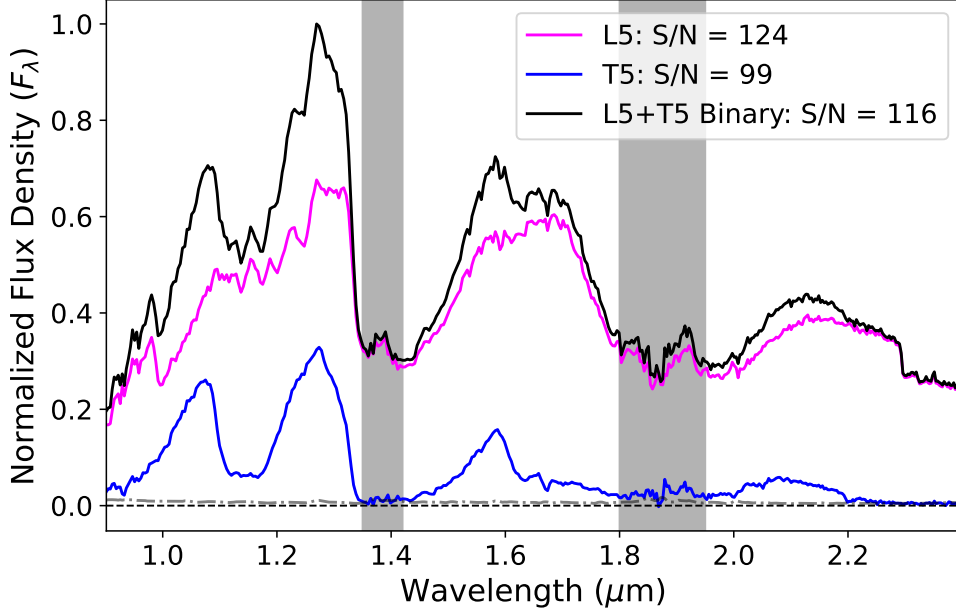


Figure 2. Example of a synthetic binary template with $S/N = 116$ (black line), constructed from a $S/N = 124$ L5 dwarf spectrum (magenta line) and a $S/N = 99$ T5 dwarf spectrum (blue line). The fluxes of the single components are scaled relative to each other using the Dupuy & Liu (2012) M_J /spectral type relation, and to the combined spectrum which is normalized between 1.20–1.35 μm . The uncertainty for the combined light spectrum is shown as a dash-dot line, and the vertical gray bands indicate regions of strong telluric absorption.

where $\sigma_S[\lambda]$ is the uncertainty spectrum of the source and α is a scaling factor that minimizes χ^2 (Cushing et al. 2005). A source was considered a spectral binary candidate if the binary template was a significantly better fit than the single template based on an F-test comparison of χ^2 values. This comparison also allowed determination of component spectral types. The B10 approach was defined for primaries classified L5–T2 and secondaries classified T2–T7, and applied to combined-light spectra with classifications of L8–T4.

B14 followed a similar procedure for late-M/early-L dwarf plus T dwarf binaries, evaluating 13 indices to define 17 selection criteria, with “strong” candidates satisfying at least eight criteria and “weak” candidates satisfying four to eight criteria. B14 also used a χ^2 template comparison to eliminate spurious candidates, particularly blue L dwarfs, and to determine component classifications. The B14 approach was defined for primaries classified M7–L7 and secondaries classified T1–T7, and applied to combined-light spectra with classifications of M7.5–L8 (Bardalez Gagliuffi et al. 2015).

We applied the B10 and B14 index criteria to the synthetic single and binary templates that matched the appropriate combined-light spectral types for the two methods. To simplify our test, we included both “weak” and “strong” binary candidates, and did not perform the χ^2 test. To assess the performance of the indices, we mea-

sured the statistics of recall (R):

$$R \equiv \frac{TP}{TP + FN} \quad (2)$$

precision (P):

$$P \equiv \frac{TP}{TP + FP} \quad (3)$$

and F1-score:

$$F1 \equiv \frac{2 \times TP}{2 \times TP + FP + FN} \quad (4)$$

where TP is the number of true positives (binary templates selected as binaries), TN is the number of true negatives (single templates rejected as binaries), FP is the number of false positives (single templates selected as binaries), and FN is the number of false negatives (binary templates rejected as binaries). Recall measures the fraction of selected binaries among true binaries, precision measures the fraction of true binaries among selected binaries, and F1-score combines these statistics. Values range from 0 to 1, with the latter indicating perfect performance.

Performance statistics as a function of combined-light spectral type are shown in Table 1. While both methods perform reasonably well in aggregate for identifying single sources (TN = 0.75 for B10, 0.95 for B14), they have relatively poor performance in identifying binary sources (TP = 0.64 for B10, 0.23 for B14). Focusing on recall (Table 2 and Figure 3), the B10 indices identify 62%–63% of true binaries, and the B14 indices identify 19%–27% of true binaries, depending on S/N. These results suggest relatively poor performance; however, in select spectral compositions performance improves considerably. For L5–T2 primaries and T2–T7 secondaries, the B10 recall increases to 0.79–0.85, while for M7–L7 primaries and T1–T7 secondaries, the B14 recall increases to 0.45–0.48, again depending on S/N. Outside these optimal combinations, and particularly for systems with equivalent component types (e.g., late-M + late-M, early-L + early-L, etc.), recall declines to $R < 0.1$.¹⁰ Hence, both approaches miss a significant fraction of binary systems when components are outside the spectral classification ranges that these methods are optimized for. Note that S/N has a minor impact on performance statistics ($\Delta R \lesssim 0.1$).

Finally, we note that it took 20.7 min to measure the indices and determine binary classifications for the 31,546 template spectra with the B10 and B14 methods on a laptop computer,¹¹ an average of 39 ms per spectrum. The original classification of templates using a χ^2 comparison was less computationally efficient, taking an average of 2.3 seconds per object.

¹⁰ One exception is early-T + early-T combinations for the B10 index method, where the rapid evolution of spectral morphologies across the range results in a relatively high recall of $R = 0.45$.

¹¹ All computations in this investigation were run on an 11th Generation Intel Core i9-11900H processor at 2.50GHz, with 16.0 GB (15.7 GB usable) RAM and a 64-bit operating system with x64-based processor.

Table 1. Performance Statistics of Index-based Methods for Spectral Binary Identification

Type	B14			B10		
	P	R	F1	P	R	F1
M8	0.69	0.11	0.18
M9	0.87	0.06	0.10
L0	0.68	0.12	0.20
L1	0.78	0.19	0.31
L2	0.83	0.14	0.24
L3	0.92	0.42	0.58
L4	0.76	0.45	0.56
L5	0.82	0.39	0.53
L6	0.89	0.18	0.29
L7	0.97	0.20	0.34
L8	0.86	0.41	0.56	0.97	0.23	0.38
L9	0.87	0.57	0.69
T0	0.75	0.77	0.76
T1	0.63	0.69	0.66
T2	0.61	0.76	0.68
T3	0.59	0.72	0.64
T4	0.97	0.16	0.27

NOTE—Performances statistics are precision (P), recall (R), and F1-score (F1). Templates satisfying both “weak” and “strong” criteria were assumed to be selected as binary candidates.

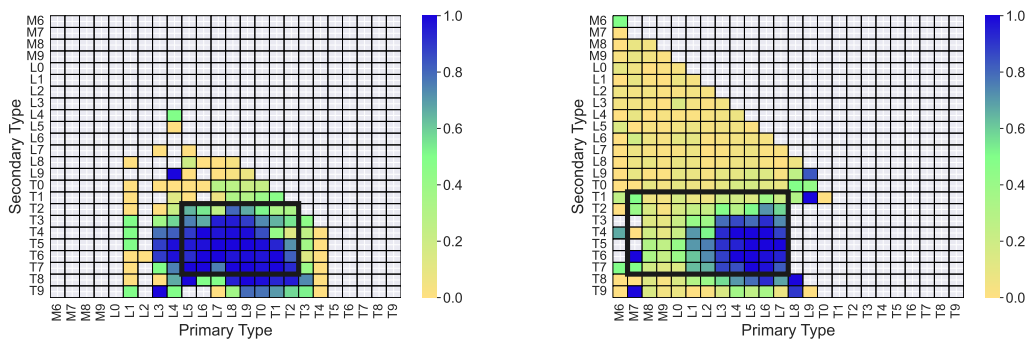


Figure 3. Recall for the index-based methods of B10 (left) and B14 (right) as a function of component classifications. Only those combinations whose combined-light spectra match the applicable spectral range of these methods (L8–T4 for B10, M8–L8 for B14; black boxes) are shown. Each box represents an average of recall across all S/N groups.

3. RANDOM FOREST MODEL DESIGN

Building on prior work (Desai et al. 2023), we evaluated a random forest model as an alternative approach to very low mass binary identification and classification. We used the `scikit-learn` package (Pedregosa et al. 2011) to implement two algorithms: a RF classifier (`RandomForestClassifier`) which returns a binary class based on the

Table 2. Recall Statistics for Index-based Methods

Binary Combination (Primary + Secondary)	B14			B10		
	low	mid	high	low	mid	high
Full Sample	0.27	0.22	0.19	0.63	0.66	0.62
M7-L7 (P) + T1-T7 (S)	0.48	0.47	0.45	0.78	0.77	0.79
L5-T2 (P) + T2-T7 (S)	0.79	0.87	0.90	0.79	0.85	0.79
late M + late M	0.14	0.01	0.01
late M + early L	0.07	0.02	0.01
late M + late L	0.08	0.05	0.01
late M + early T	0.20	0.11	0.07
late M + late T	0.21	0.12	0.16
early L + early L	0.12	0.01	0.01
early L + late L	0.12	0.03	0.03
early L + early T	0.40	0.37	0.37	0.70	0.66	0.69
early L + late T	0.47	0.48	0.62	0.74	0.90	0.83
late L + late L	0.13	0.05	0.03	0.11	0.00	0.00
late L + early T	0.55	0.55	0.50	0.76	0.77	0.74
late L + late T	0.69	0.75	0.97	0.86	0.90	1.00
early T + early T	0.46	0.52	0.45
early T + late T	0.66	0.69	0.76

NOTE—Spectral type groupings are as follows: late-M = M6–M9, early-L = L0–L4, late-L = L5–L9, early-T = T0–T4, and late-T = T5–T9. Templates satisfying both “weak” and “strong” criteria were assumed to be selected as binary candidates. Only spectral type groupings with more than 10 templates are included.

majority outcome of decision trees, and a RF regressor (`RandomForestRegressor`) which returns a numerical value based on the average across decision trees. Our models used the normalized flux points of the spectra and additional quantities computed from them (see below) as features, and return a decision on whether a source is a binary (classifier) and the component classifications (classifier and regressor).

Table 3 summarizes the parameters for the architecture of our random forest models. For most parameters, we used default values defined in the `scikit-learn` package, but optimized four parameters via iterative tuning: the number of estimators (`n_estimators`), equal to the total number of decision trees in the RF model; the maximum depth (`max_depth`) of each decision tree; the minimum number of samples used to split a leaf node (`min_samples_split`); and the minimum samples per leaf (`min_samples_leaf`), which determines when a decision tree branch ends. These parameters were optimized using the F1-score (Eqn. 4). We found that `n_estimators` and `max_depth` had the largest impact on the F1-score, with larger values of each yielding larger F1-scores, albeit at a computational cost of training more decision trees. We also found that smaller `min_samples_split` and `min_samples_leaf` improved F1-scores slightly. We therefore chose parameter values of `n_estimators` = 50, unlimited `max_depth`, `min_samples_split` = 2, and `min_samples_leaf` = 2.

Table 3. Random Forest Model Parameters

Parameter	Description	Adopted Values	
		Classifier	Regressor
<code>n_estimators</code>	Number of trees in the forest	50	50
<code>max_depth</code>	Maximum number of nodes in a tree	No limit	No limit
<code>min_samples_split</code>	Minimum number of samples to divide a node	2	2
<code>min_samples_leaf</code>	Minimum required samples at a leaf node	2	2
<code>max_leaf_nodes</code>	Maximum number of leaves in a node	None	None
<code>max_features</code>	Maximum number of nodes considered when finding the best node division	<code>sqrt</code>	all
<code>criterion</code>	Evaluate the quality of the division of a node by minimizing a loss function	<code>gini</code>	<code>squared_error</code>
<code>min_weight_fraction_leaf</code>	Minimum fraction of weights required at each node	None	None
<code>min_impurity_decrease</code>	a Node division only occurs if the decrease in impurity is greater than this value	0	0
<code>bootstrap</code>	Whether a random subsample from the larger dataset is chosen when building trees	True	True
<code>oob_score</code>	Metric for calculating the out-of-bag (oob) score that evaluates performance of a tree	<code>accuracy_score</code>	<code>r2_score</code>
<code>n_jobs</code>	Number of CPU cores	None	None
<code>warm_start</code>	Whether to use the previous solution to fit the forest	False	False
<code>class_weight</code>	Weights for each class	None	-
<code>ccp_alpha</code>	Parameter that controls pruning; 0 implies no pruning	0	0
<code>max_samples</code>	Number of samples to train each base estimator	<code>n_samples</code>	<code>n_samples</code>
<code>monotonic_cst</code>	Monotonicity constraint on features; None implies no constraint	None	None

3.1. Binary Identification Models

For our binary identification model (BI_d), we explored eight variations of RF models for each spectral S/N range (Table 4). Our baseline model BI_{d1} used the 409 flux points in the wavelength range 0.9–2.4 μm as input features. Model BI_{d2} included an additional 409 flux points of the difference spectrum between the input spectrum and its best-fit single template (Section 2.4), for a total of 818 flux features. Model BI_{d3} used the input spectrum after masking out regions of strong telluric absorption over 1.35–1.42 μm and 1.80–1.95 μm , resulting in 351 flux features. Model BI_{d4} combined the flux samples from models BI_{d2} and BI_{d3}, resulting in 702 flux features. Models BI_{d5} and BI_{d6} were trained on a subset of templates encompassing the spectral type ranges examined in B14, primary types M7–L7 and secondary types T1–T7, with data prepared as in models BI_{d1} and BI_{d2}. Models BI_{d7} and BI_{d8} were trained on a subset of templates encompassing the spectral type ranges examined in B10, primary types L5–T2 and secondary types T2–T7, again with data prepared as in models BI_{d1} and BI_{d2}. These last four models aimed to assess whether the RF models achieved better performance in the specific binary compositions explored in the index-based

Table 4. Binary Identification (BI) Models

Model	Binary	Difference	Telluric	Training
Name	SpTs	Flux	Masking	Time (sec)
BI1	M6-T9	No	No	5.2
BI2	M6-T9	Yes	No	7.5
BI3	M6-T9	No	Yes	4.9
BI4	M6-T9	Yes	Yes	6.8
BI5	M7-L7 (P) T1-T7 (S)	No	No	2.6
BI6	M7-L7 (P) T1-T7 (S)	Yes	No	3.6
BI7	L5-T2 (P) T2-T7 (S)	No	No	1.6
BI8	L5-T2 (P) T2-T7 (S)	Yes	No	2.7
BI9	M6-T9 ^a	No	No	5.2

^aThis model accounts for uncertainties in the absolute magnitudes of individual components by accounting for the 0.4 mag systematic uncertainty in the Dupuy & Liu (2012) M_J /spectral type relation.

studies. Finally, model BI9 replicates BI1 but examines the impact of systematic uncertainty in the Dupuy & Liu (2012) M_J /spectral type relation, by scaling the component spectra with magnitudes drawn from the relation value plus a 0.4 mag random gaussian uncertainty. Each model and S/N sample was trained using 70% of our single and binary templates selected randomly, and tested on the remaining 30% of the templates. Training times were consistently under 10 s for each model.

3.2. Component Classification Models

Our second class of models determined the spectral classifications of the primary and secondary stars within a binary system, for which we used the `scikit-learn MultiOutputRegressor` model. This implementation extends the functionality of single-output regressor models to allow for multiple outputs, with each output variable treated independently during training. As with our BI models, we explored eight different sets of models (BClass) for each S/N sample based on the input features (inclusion of difference spectrum, full or telluric masked input spectrum) and constraints on the binary compositions, and each model was trained and tested on 70% and 30% of the binary templates, respectively. Training times were longer for these models, but were still under 20 s for all cases explored.

3.3. Feature Importance

In addition to accurate identification and classification of binary spectra, we also sought to identify the spectral features that indicate the presence of an unresolved companion. The RF model enables this assessment through feature importance (FI), which quantifies the contribution of each feature to the performance of the model. In `scikit-learn`, FI is calculated using the mean decrease in impurity (MDI) when a feature is used to split a node. For our binary identification model, impurity is mea-

Table 5. Binary Subtype Classification (BClass) Models

Model	Binary	Difference	Telluric	Training
Name	SpTs	Flux	Masking	Time (sec)
BClass1	M6-T9	No	No	9.0
BClass2	M6-T9	Yes	No	18
BClass3	M6-T9	No	Yes	8.0
BClass4	M6-T9	Yes	Yes	16
BClass5	M7-L7 (P) T1-T7 (S)	No	No	2.4
BClass6	M7-L7 (P) T1-T7 (S)	Yes	No	4.5
BClass7	L5-T2 (P) T2-T7 (S)	No	No	1.3
BClass8	L5-T2 (P) T2-T7 (S)	Yes	No	2.4

sured using the Gini index; for our binary classification model, impurity is measured using mean squared error.

4. MODEL PERFORMANCE

4.1. Binary Identification

Table 6 summarizes the cumulative precision, recall, and F1-score performance for each of the nine binary identification models and three S/N groups (27 models total), while Figures 4 and 6 display the receiver operating characteristic (ROC; Peterson et al. 1954) curves and confusion matrices for these models. All models showed exceptional performance, with precisions ≥ 0.85 , recall ≥ 0.75 , and F1-scores ≥ 0.84 ; the majority of models had performance metrics >0.9 . The baseline model, BId1, had a precision, recall, and F1-score of 0.91, 0.86, and 0.88 respectively, averaged across S/N groups. Notably, performance metrics are inversely correlated with S/N, with the lowest S/N group showing the best performance. The best overall performance is seen in the BId7 and BId8 models, based on the “optimal” spectral compositions for spectral binaries studied in B10, with all three metrics being $\gtrsim 0.9$ for the mid- and high-S/N templates. The BId9 model, which accounts for variance in component absolute brightness, shows only slightly worsened performance (1–2%) compared to our baseline model, indicating that absolute brightness variance is not a major factor in binary identification. The excellent performance of all of the models can be seen in the ROC curves, which show that beyond decision tree selection thresholds of 0.5 the models achieve $>80\%$ true positive rates while maintaining $<5\%$ false positive rates. The areas under the curve (AUCs), a common performance metric for ROC curves, are ≥ 0.95 for all but the BId2 model.

Figure 6 displays the recall performance of the BId1 binary identification model decomposed across all combinations of primary (P) and secondary (S) component types. The B10 range ($P \in \{L5, T2\}$, $S \in \{T2, T7\}$) have recall values close to unity, while binaries with equal component types (diagonal axis), those with a T8-T9 secondary,

Table 6. Precision (P), Recall (R), and F1-score for Binary Identification Models

Model	S/N	P	R	F1	# Singles	# Binaries	Unc.
BId1	low	0.98	0.89	0.93	1827	1773	0.02
BId1	mid	0.86	0.82	0.84	1827	1773	0.02
BId1	high	0.85	0.88	0.87	1552	1484	0.03
BId2	low	0.94	0.88	0.91	1827	1773	0.02
BId2	mid	0.84	0.83	0.84	1827	1773	0.02
BId2	high	0.86	0.89	0.87	1552	1484	0.03
BId3	low	0.99	0.89	0.93	1827	1773	0.02
BId3	mid	0.86	0.84	0.85	1827	1773	0.02
BId3	high	0.85	0.88	0.87	1552	1484	0.03
BId4	low	0.95	0.87	0.91	1827	1773	0.02
BId4	mid	0.84	0.83	0.84	1827	1773	0.02
BId4	high	0.86	0.89	0.87	1552	1484	0.03
BId5	low	0.99	0.85	0.92	1798	506	0.04
BId5	mid	0.94	0.71	0.81	1798	506	0.04
BId5	high	0.91	0.75	0.82	1523	427	0.05
BId6	low	1.00	0.84	0.91	1798	506	0.04
BId6	mid	0.93	0.70	0.80	1798	506	0.04
BId6	high	0.90	0.75	0.82	1523	427	0.05
BId7	low	1.00	0.88	0.93	1804	284	0.06
BId7	mid	1.00	0.89	0.94	1804	284	0.06
BId7	high	1.00	0.96	0.98	1534	224	0.07
BId8	low	0.98	0.83	0.90	1804	284	0.06
BId8	mid	1.00	0.91	0.95	1804	284	0.06
BId8	high	0.99	0.97	0.98	1534	224	0.07
BId9	low	0.98	0.87	0.93	1827	1773	0.02
BId9	mid	0.85	0.82	0.83	1827	1773	0.02
BId9	high	0.84	0.87	0.85	1827	1773	0.02

NOTE—Uncertainty (Unc.) on statistics is based on the Poisson counting uncertainty of the smaller of the number of synthetic single and binary templates.

or those with T5 or later primaries have the smallest recall values of $\lesssim 0.5$. These regions encompass component compositions where spectral peculiarities are minimal in the combined light spectrum. Notably, these metrics are both superior to and cover a broader range of spectral type combinations than the index-based methods of B10 and B14 (Figure 3). More importantly, the speed of classification is more than an order of magnitude faster than the index method. The test sample was classified at a rate of 441 spectra/second, or 2 ms per spectrum, compared to 39 ms per spectrum for the index methods.

We conducted a similar analysis on our alternative models. Incorporating the difference flux (BId2 and BId4) or masking the telluric absorption regions (BId3 and BId4) did not significantly improve model recall over our baseline model BId1, even when broken down by component spectral types. Models trained on templates encompassing the spectral type ranges used in the B10 and B14 studies (BId5–8) clearly

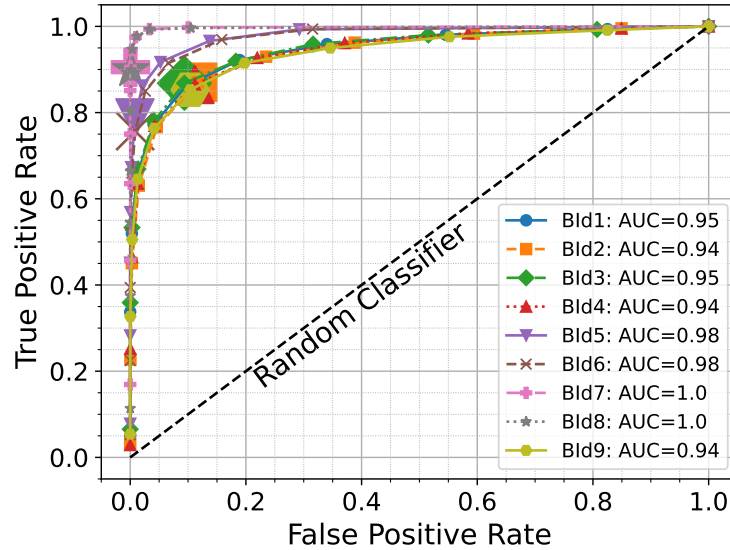


Figure 4. Receiver operating characteristic (ROC) curves for the nine binary identification (BId) models examined in this study, comparing the true positive rate (true binaries) to the false positive rate (singles identified as binaries) as a function of detection threshold. The threshold for binary identification, computed as the fraction of decision trees identifying a spectrum as binary, was allowed to vary from 0 to 1. Random selection would follow the dashed line, while the computed curves indicate high fidelity in identifying true binaries. The legend indicates the color, point style, and line style corresponding to the given BId model, and lists the area under the curve (AUC) metric for each model. Larger symbols correspond to a detection threshold of 0.5, corresponding to majority vote.

		Predicted				Predicted				Predicted	
		Single	Binary			Single	Binary			Single	Binary
Actual	Bld1	0.90 (4703)	0.10 (503)	Actual	Bld2	0.88 (4598)	0.12 (608)	Actual	Bld3	0.91 (4718)	0.09 (488)
	Single	0.14 (692)	0.86 (4338)		Binary	0.13 (652)	0.87 (4378)		Binary	0.13 (664)	0.87 (4366)
Actual	Bld4	0.89 (4624)	0.11 (582)	Actual	Bld5	0.99 (5092)	0.01 (42)	Actual	Bld6	0.99 (5090)	0.01 (44)
	Single	0.13 (677)	0.87 (4353)		Binary	0.21 (277)	0.79 (1027)		Binary	0.24 (317)	0.76 (987)
Actual	Bld7	1.00 (5140)	0.00 (2)	Actual	Bld8	1.00 (5135)	0.00 (7)	Actual	Bld9	0.90 (4666)	0.10 (540)
	Single	0.09 (75)	0.91 (717)		Binary	0.10 (80)	0.90 (712)		Binary	0.15 (739)	0.85 (4291)

Figure 5. Confusion matrices for each of the nine binary identification (BId) models examined in this study, comparing actual binary status (rows) with predicted binary status (columns). Numbers in each square panel indicate the fraction and number of templates corresponding to each condition, while the shading indicates the fraction along a row from 0% (white) to 100% (black).

outperform the index-based methods. The BId5 model shows a nearly factor of 4 improvement in recall as compared to the B14 index method, 0.60 versus 0.16 averaged over all relevant combinations and S/N values; while the BId7 model had modestly higher recall compared to the B10 index method, 0.59 versus 0.56 (Figure 7). How-

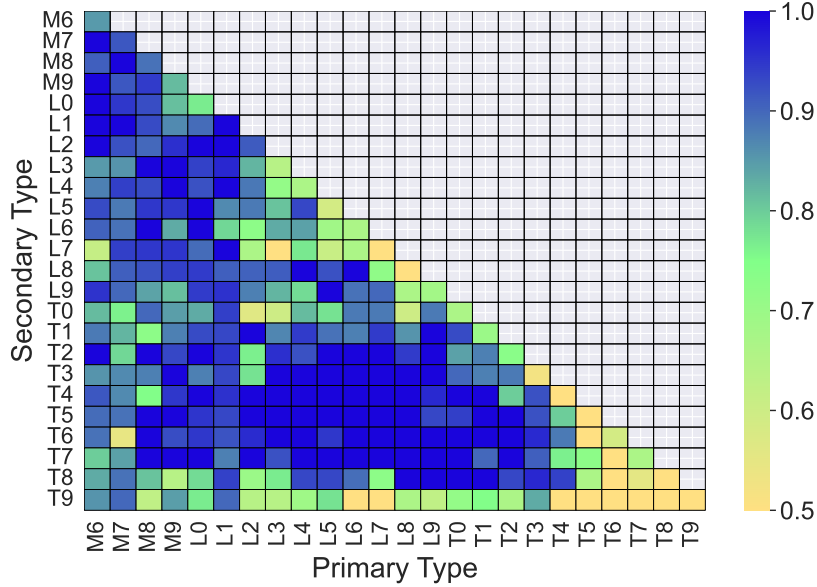


Figure 6. Recall for the BI d1 model for all spectral type combinations used for our synthetic binaries. Values represent the cumulative recall across all S/N ranges. Note that the color scale is narrowed to span values of 0.5–1.0.

ever, these specialized models still underperformed relative to the BI d1 model, even within their respective training ranges. Regions with high recall in the specialized models were already well-classified by BI d1, resulting in no substantial gain in performance.

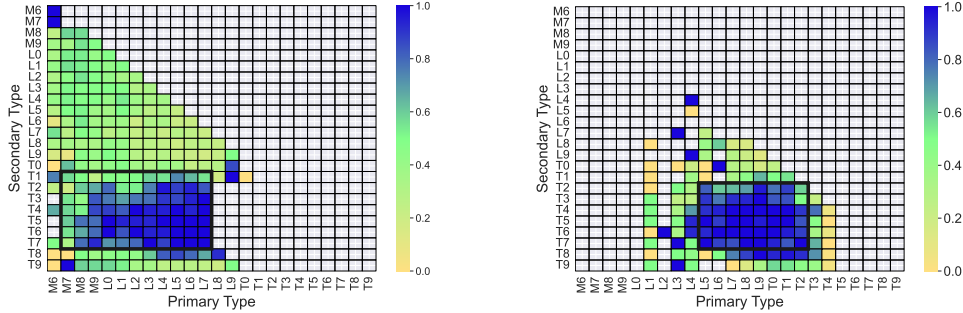


Figure 7. Recall for the BI d5 model (left) and the BI d7 model (right) for all spectral type combinations used for our synthetic binaries. Values represent the cumulative recall across all S/N ranges. Note that the color scale spans values of 0.0–1.0, broader than the range shown in Figure 6.

Figure 8 displays feature importance as a function of wavelength on both linear and log scales for the BI d1 model across the three S/N categories, compared to an L5 plus T5 binary combination to associate FI peaks to spectral features. For the low S/N case, FI has a strong peak at $1.274 \mu\text{m}$, extending around the *J*-band flux peak for T dwarfs. Indeed, the logarithmic scaling of FI resembles the spectral structure of a

T dwarf. We interpret this structure as the RF algorithm focusing on the emission features of T dwarf companions, as the S/N is too low to clearly distinguish absorption features from a faint companion. In contrast, the high S/N FI shows more structure across the spectral band, and is more tuned to the absorption features present in L and T dwarf spectra, including the K I lines at $1.25 \mu\text{m}$, CH_4 molecular structure at $1.67 \mu\text{m}$ and $2.25 \mu\text{m}$, and the CO band at $2.32 \mu\text{m}$. The presence of significant structure in the FI distribution at the wavelengths of these features indicates that the binary model may be more selective of systems with late-L and T dwarf secondaries, likely due to their distinct spectral features as compared to late-M and early-L dwarfs.

4.2. Component Classification

Table 7 summarizes the performance of our binary component classification model, quantified by the difference (Δ) and standard deviation (σ_Δ) between the input and output primary and secondary classifications, averaged across the test data. We also provide estimates of the uncertainties on these values assuming Poisson counting statistics based on the number of synthetic binary spectra. The classification of all 25,684 binaries in the test sample took 162 s, or 6 ms per spectrum.

For all of the model and S/N groups, we find excellent agreement among the primary classifications, with absolute median classification errors of $\lesssim 0.1$ subtypes and typical standard deviations of $\lesssim 0.5$ subtypes. We also find small median classification errors for the secondary types, but higher standard deviations of $\lesssim 1$ subtype. In nearly all cases, performance improves for the higher S/N groups, particularly for primary classification. We see minimal improvement in performance when difference flux or telluric masking is included (BClass2-4), indicating that neither contributes significantly to determining component types. However, there are notable improvements in performance for models based on the B10 and B14 subtype pairings (BClass5 and BClass7), for which standard deviations of secondary classifications decrease by a factor of two to $\lesssim 0.5$ subtypes.

Figure 9 displays the distribution of median classification errors, standard deviations, and recall as a function of paired component types for the BClass1 model. Here, recall is defined as inferred spectral types being within one subtype of the input classification. Primary classifications are nearly perfect for all spectral type combinations, with modest deviations (≈ 1 subtype) for systems with mid-type L dwarf and L/T transition primaries. The performance for secondary classification shows greater scatter, with significant skew (by up to ~ 4 subtypes) toward later secondary types, likely due to the minimal contribution of the secondaries to the combined light spectrum. A similar large skew is seen for late-M/L dwarf binaries with similar component classifications, likely due to similarities in spectral shape. We also see significant variance ($\sigma_\Delta \sim 2$ subtypes) among secondary classifications for systems with late-M or early-L primaries. On the other hand, a wide range of systems with T

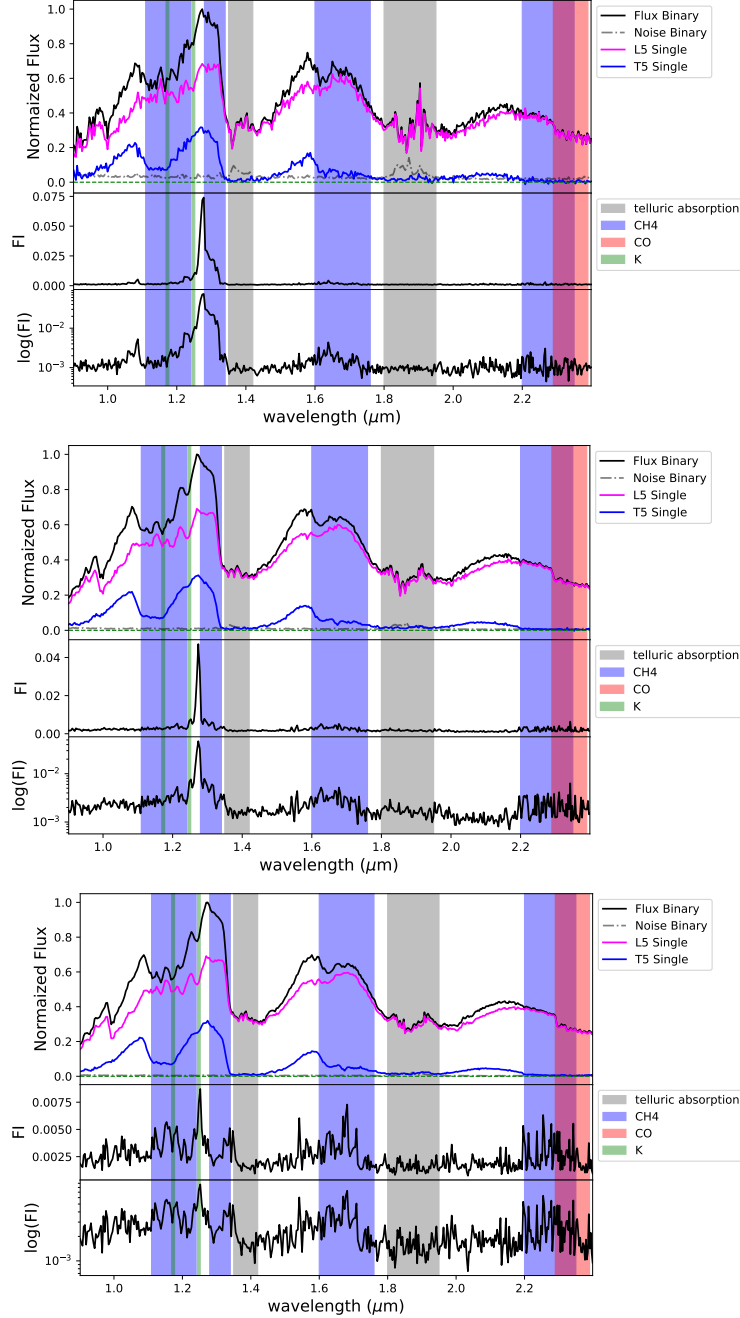


Figure 8. Feature importance (FI) for the BId1 model for low (top), mid (middle) and high (bottom) S/N groups. Each panel displays FI on linear (middle plot) and logarithmic scales (bottom plot), compared to an example of an L5 plus T5 binary spectrum with a S/N in the associated range (top plot). Regions associated with telluric (grey), K I (green), CH₄ (blue) and CO (red) absorption are indicated by vertical bands.

dwarf secondaries are accurately classified, with secondary classification recall $\gtrsim 0.8$ and scatter < 1 subtype.

As with the binary identification models, incorporating difference spectra or masking telluric regions had no significant impact on the performance of primary or secondary classification compared to our baseline BClass1 model. The B10- and B14-based

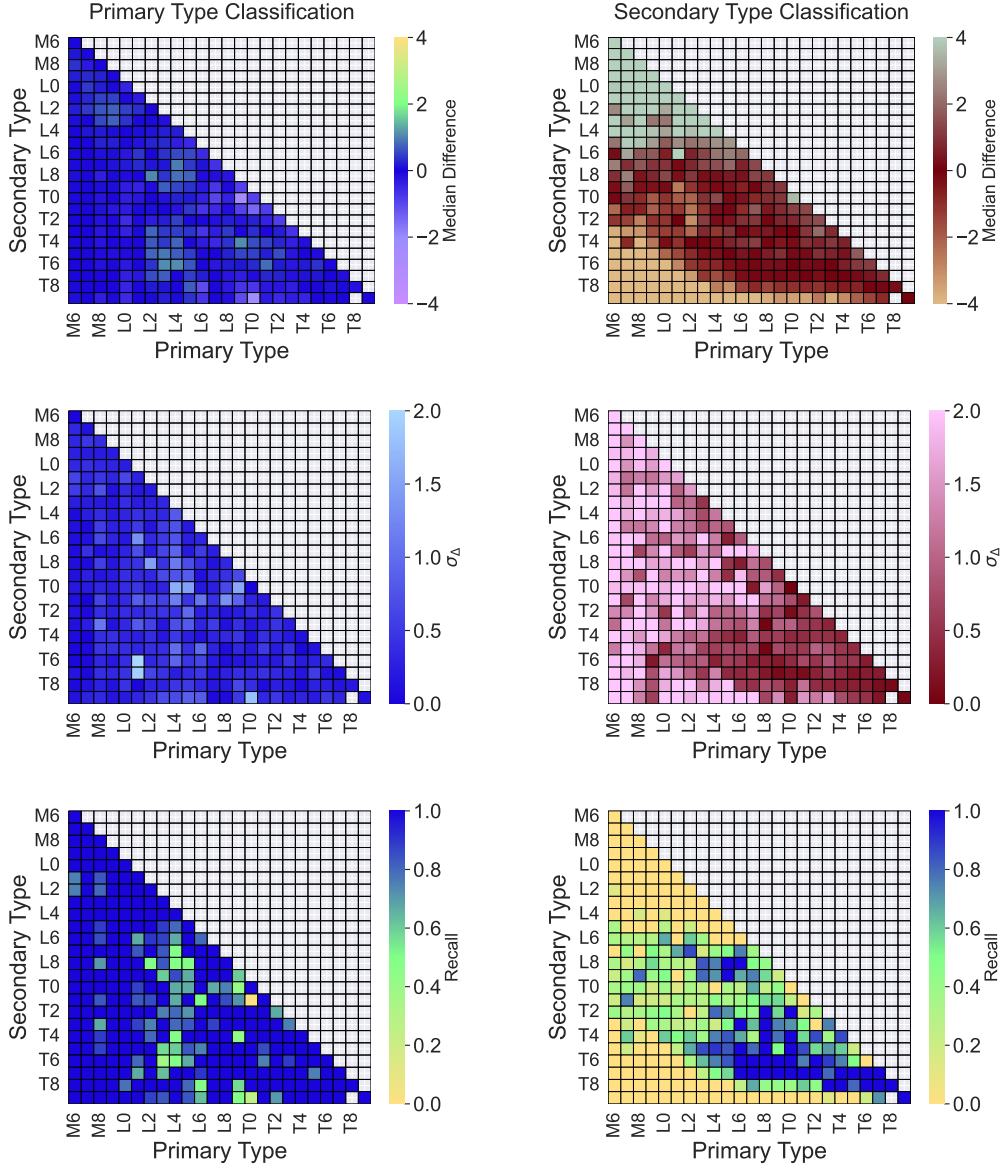


Figure 9. Median classification error (top panels), standard deviations (middle panels), and recall (bottom panels) for primary (left) and secondary (right) classification as a function of component type combination for the BClass1 model and mid-S/N group. Classification differences were calculated as predicted minus true. Recall is defined here as the percentage of sources classified within 1 subtype of their true values.

models (BClass5-8) have similar measures of error and scatter as BClass1 for primary classifications, but yield a 2–4 \times improvement in the classification of the secondary component ($\sigma_{\Delta} = 0.5$ –0.6 subtypes for BClass5 and BClass6, $\sigma_{\Delta} = 0.2$ –0.6 subtypes for BClass7 and BClass8), likely due to the prevalence of binaries with distinct component spectral types among the templates in the training and testing data.

Figure 10 displays feature importance for the BClass1 model for our three S/N groups, again compared to a spectrum of an L5 plus T5 synthetic binary to guide feature identification. FI distributions for primary and secondary are distinct and

Table 7. Classification Errors and Standard Deviations for Binary Classification Models

Model	S/N	Primary		Secondary		# Binaries	Unc.
		Δ	σ_{Δ}	Δ	σ_{Δ}		
BClass1	low	-0.14	0.73	-0.10	1.00	1800	0.02
BClass1	mid	-0.03	0.35	+0.01	1.00	1800	0.02
BClass1	high	-0.02	0.27	-0.07	0.93	1518	0.03
BClass2	low	-0.14	0.74	-0.14	1.10	1800	0.02
BClass2	mid	-0.03	0.35	-0.00	1.00	1800	0.02
BClass2	high	-0.03	0.28	-0.05	0.90	1518	0.03
BClass3	low	-0.14	0.74	-0.09	1.00	1800	0.02
BClass3	mid	-0.03	0.35	-0.01	1.00	1800	0.02
BClass3	high	-0.03	0.28	-0.07	0.92	1518	0.03
BClass4	low	-0.14	0.73	-0.15	1.10	1800	0.02
BClass4	mid	-0.04	0.35	-0.02	1.00	1800	0.02
BClass4	high	-0.04	0.29	-0.05	0.91	1518	0.03
BClass5	low	-0.10	0.70	+0.05	0.59	462	0.05
BClass5	mid	-0.02	0.35	-0.03	0.52	462	0.05
BClass5	high	-0.02	0.34	+0.07	0.45	396	0.05
BClass6	low	-0.08	0.70	+0.02	0.59	462	0.05
BClass6	mid	-0.02	0.33	-0.04	0.56	462	0.05
BClass6	high	-0.01	0.32	+0.04	0.45	396	0.05
BClass7	low	-0.01	0.44	-0.03	0.58	288	0.06
BClass7	mid	+0.01	0.34	-0.03	0.51	288	0.06
BClass7	high	-0.00	0.21	-0.00	0.23	240	0.06
BClass8	low	-0.03	0.43	-0.01	0.59	288	0.06
BClass8	mid	+0.011	0.32	-0.01	0.50	288	0.06
BClass8	high	-0.03	0.21	+0.01	0.22	240	0.06

NOTE—Median error Δ is defined as true classification minus predicted classification. Both classification errors and standard deviations (σ_{Δ}) are computed across all spectral type combinations within the template spectral type range for each model. Uncertainties (Unc.) on these statistics are based on Poisson counting uncertainty of the number of binary spectra in the sample.

evolve with S/N group. For the low S/N group, the primary classification FI shows spikes in the 1.10-1.24 μm region that encompasses both CH_4 and K I absorption features, and at the interface of the CH_4 and CO bands at 2.2 and 2.3 μm . The secondary classification FI also shows features in the 1.10-1.24 μm region, as well as at the 1.33 μm edge of the strong $\text{CH}_4/\text{H}_2\text{O}$ band, and in the 1.6 μm CH_4 band. These features are also present in the mid and high S/N groups, but become more concentrated at 1.12 μm for primary classification and at 1.25 μm for secondary classification. A new feature emerges in the primary FI for the mid- and high-S/N models at 1.95 μm , in the region of strong H_2O absorption and at the edge of the

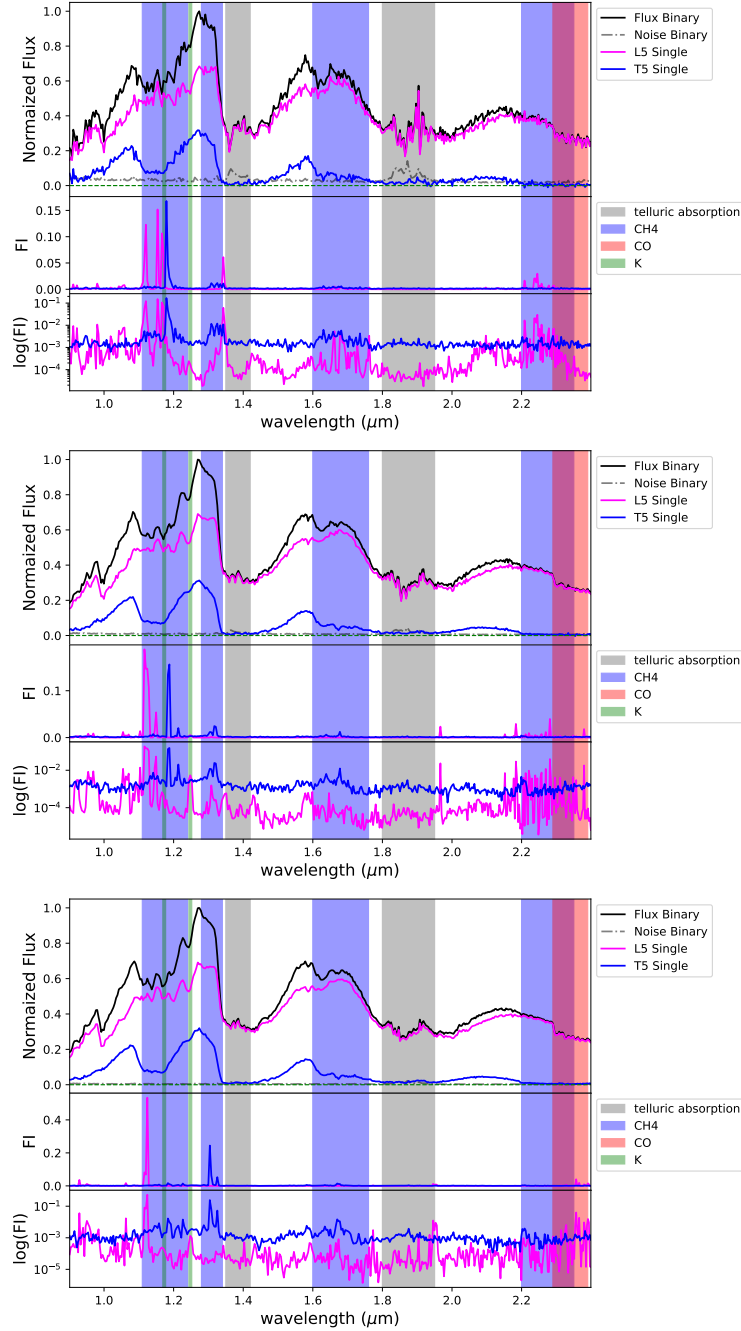


Figure 10. Feature importance (FI) for the BClass1 model for low (top), mid (middle) and high (bottom) S/N groups (cf. Figure 8). Each panel displays FI for primary (magenta) and secondary (blue) classification on linear (middle plot) and logarithmic scales (bottom plot), compared to an L5 plus T5 synthetic binary spectrum with a S/N in the associated range (top plot). Regions associated with telluric (grey), K I (green), CH₄ (blue) and CO (red) absorption are indicated by vertical bands.

1.80-1.95 μm telluric band. Beyond these spikes, the FI spectra are relatively flat across other wavelengths.

5. APPLICATION TO KNOWN BINARY SPECTRA

Our analysis of synthesized binary spectra indicates robust determination of both unresolved binarity and component classifications spanning a wide range of very low mass dwarf component types. However, internal validation must be supported by analysis of actual binary spectra. We curated a sample of known VLM binary spectra for sources with primary or combined-light classifications of M7 from the Ultracool-Sheet (Best et al. 2024) which have been confirmed by resolved imaging, astrometric variability, or radial velocity variability. Of 176 known binary systems, 43 have low-resolution IRTF/SpeX spectra available in the SPLAT database with resolved or combined-light spectroscopy (Table 8). The sources have primary spectral types spanning M8 to T8.5 and secondary spectral types spanning L1.5 to T9.5. We evaluated the binary selection indices for those sources that meet the B10 and B14 index-based selection criteria, encompassing 14 and 25 of these binaries, respectively. We focused our evaluation on the correct identification and classification of these binaries (recall) for models 1, 5, and 7, using the models trained to the appropriate spectral data S/N.

Table 8. Random Forest Analysis of Confirmed Ultracool Dwarf Binaries

Name	Method ^a	Combined Light		Index Class		Binary Identification		BClass1		BClass5		BClass7		Ref	
		Type	S/N	B14	B10	Bid1	Bid5	Bid7	P	S	P	S	P		S
SDSS J000649.16-085246.3	SP, SB1	M8.0	high	strong	...	b	s	...	M7.5	T0.6	M7.8	T5.2	L8.1	T3.3	15
2MASS J01303563-4445411	V	M9.0	high	single	...	s	s	...	M8.9	T0.4	M9.0	T3.7	L6.2	T3.4	20
2MASSW J0320284-044636	SP, SB1	M8.0	high	strong	...	b	s	...	M8.1	T3.7	M8.3	T5.4	L8.1	T3.4	9
SDSS J034408.91+0111124.9	SP, A	L0.0	high	weak	...	b	s	...	L0.6	T3.1	L0.9	T4.6	L8.1	T3.3	3,4
DENIS-P J035726.9-441730	V	M9	mid	single	...	b	s	...	L1.5	L5.3	L1.8	T1.9	L6.0	T2.8	3,31
SDSSp J042348.57-041403.5	SP, V	T0.0	mid	...	weak	b	...	b	L9.0	T1.9	L4.9	T2.2	L6.7	T2.1	18,21
WISEPA J045853.89+643452.9	V	T8.0	low	s	T8.0	T8.2	L5.9	T5.3	T1.7	T5.8	30,14
2MASS J05185995-2828372	SP, V	L8.0	mid	weak	strong	b	b	b	L7.1	T5.6	L6.8	T5.5	L7.0	T5.5	18,21
2MASS J05431887+6422528	V	L2.0	high	single	...	b	s	...	L1.5	L7.9	L1.7	T1.5	L5.8	T2.7	3,19
WISEPA J061135.13-041024.0	V	T0.0	low	...	strong	b	...	s	L9.4	T2.8	L5.0	T3.9	L8.6	T2.8	26,24
WISE J072003.20-084651.2	SP, V, SB1	M9.0	high	single	...	b	b	...	M9.4	T4.8	M9.8	T4.6	L6.2	T3.6	16
SDSS J080531.84+481233.0	SP, A, SB1	T0.0	low	...	weak	s	...	s	L3.6	T4.7	L3.5	T5.3	L7.3	T3.8	17,21
DENIS-P J0823031-491201	A	L1.0	high	single	...	b	s	...	L1.2	L6.6	L1.5	T2.1	L5.9	T3.6	3,34
2MASSW J0850359+105716	V	L7.0	mid	single	...	b	s	...	L6.4	L9.8	L6.7	T1.6	L6.4	T2.4	13,21
SDSSp J092615.38+584720.9	SP, V	T4.0	mid	...	single	b	...	s	T4.0	T6.4	L6.5	T5.4	T1.7	T5.4	11,21
2MASSI J1017075+130839	V	L2.0	high	single	...	s	s	...	L1.6	L6.6	L1.8	T1.7	L5.9	T2.8	3,21
SDSS J102109.69-030420.1	SP, V	T3.0	mid	...	strong	b	...	b	T1.7	T5.1	L6.2	T5.5	T1.4	T5.1	7,21
SDSS J105213.51+442255.7	V, A	L9.0	mid	...	single	b	...	b	L6.7	T2.0	L6.7	T2.1	L6.4	T2.7	9,22
2MASS J11061197+2754225	SP, SB1	T2.0	high	...	weak	b	...	b	T0.7	T3.9	L5.9	T4.5	T0.5	T3.6	29,11
2MASS J11193254-1137466	V	L7.0	low	single	...	s	s	...	L7.0	T4.4	L6.8	T3.5	L7.0	T4.3	25,5
2MASSW J1146345+223053	V	L3.0	high	single	...	b	s	...	L2.1	L5.7	L2.4	T1.5	L6.2	T2.5	11,21
2MASSW J1207334-393254	V	M8.0	high	single	...	s	s	...	M7.5	L5.2	M8.0	T3.7	L6.3	T3.4	28,2
2MASS J12095613-1004008	SP, V	T3.0	low	...	weak	s	...	s	T2.2	T6.6	L5.8	T5.4	T1.8	T5.7	6,21
2MASS J12255432-2739466	V	T6.0	high	s	T5.4	T7.0	L6.5	T4.7	T1.7	T5.8	6,21
DENIS-P J122813.8-154711	V	L4.0	mid	single	...	b	b	...	L4.3	L9.9	L4.6	T1.3	L5.9	T2.0	11,21

Table 8 continued on next page

Table 8 (continued)

Name	Method ^a	Prior		Combined Light		Index Class		Binary Identification		Bclass1		Bclass5		Bclass7		Ref	
		P	S	Type	S/N	B14	B10	BId1	BId5	BId7	P	S	P	S	P		S
2MASS J1315309-264951	SP, V	L3.5	T7	L5.0	mid	strong	...	b	s	...	L5.6	T5.1	L5.8	T1.4	L6.3	T2.4	12
2MASS J1341160-3052505	SP, V	L2.5	T6.0	L2.0	high	weak	...	b	s	...	L1.9	T2.2	L1.8	T3.6	L6.4	T2.8	3,4
2MASS J14044941-3159329	SP, V	L9	T5	T2.0	mid	...	strong	b	...	b	T0.6	T3.9	L6.3	T5.4	T0.8	T4.0	29,21
SDSS J151114.66+060742.9	SP, V	L5	T5	T0.0	low	...	strong	b	...	b	L7.2	T5.5	L5.7	T5.4	L6.9	T5.0	17,4
2MASS J15200224-4422419	V	L1.5	L4.5	L1.0	high	single	...	s	s	...	L1.6	T0.0	L1.3	T2.6	L5.8	T3.0	8
SDSS J153417.05+161546.1	SP, V	T0	T5.5	T3.0	low	...	strong	b	...	b	T1.4	T6.5	L5.9	T5.4	T1.3	T6.2	17,21
2MASS J1534498-295227	V	T4.5	T5	T5.0	high	s	T4.7	T5.3	L6.5	T4.6	T1.8	T5.7	11,21
2MASS J15500845+1455180	V	L3.5	L4	L2.0	high	single	...	s	s	...	L2.4	L5.7	L2.2	T1.4	L6.0	T2.7	9,10
2MASS J1553022+153236	V	T6.5	T7.5	T7.0	high	s	T7.0	T7.7	L6.5	T4.7	T1.7	T5.7	11,21
2MASS J17072343-0558249	V	M9	L3	L1.0	low	single	...	s	s	...	L1.9	L7.1	L2.0	T1.4	L5.8	T2.5	32
WISEPA J171104.60+350036.8	V	T8	T9.5	T7.0	low	s	T7.6	T8.5	L5.7	T5.2	T1.7	T6.0	26,27
2MASSW J1728114+394859	V	L5	L7	L7.0	mid	single	...	s	s	...	L6.4	T0.3	L5.9	T2.2	L6.5	T2.4	37,21
2MASS J20261584-2943124	SP, A	L0.5	T6	L1.0	high	weak	...	s	b	...	L1.0	T4.0	L1.0	T5.6	L6.0	T3.6	35,23
SDSS J205235.31-160929.8	SP, V	L8.5	T1.5	T1.0	low	...	weak	s	...	s	L9.9	T1.9	L4.3	T3.9	L9.4	T2.7	17,21
2MASSW J2101154+175658	V	L7	L8	L5.0	low	single	...	s	s	...	L7.1	L9.3	L6.8	T2.2	L6.8	T2.5	17,21
2MASS J21321145+1341584	V, A	L4.5	L8.5	L6.0	mid	single	...	b	s	...	L6.0	L7.9	L4.9	T2.4	L6.5	T2.4	36,21
SDSSp J224953.45+004404.2	V	L3	L5	L7.0	mid	single	...	b	s	...	L6.7	L8.5	L5.8	T2.2	L6.6	T2.7	9,1
DENIS-P J225210.73-173013.4	V	L4.5	T3.5	T0.0	high	...	weak	b	...	s	L7.9	T2.4	L3.2	T4.8	L9.4	T3.4	33,21

Table 8 continued on next page

Table 8 (*continued*)

Name	Method ^a	Prior		Combined Light		Index Class		Binary Identification		BClass1		BClass5		BClass7		Ref
		P	S	Type	S/N	B14	B10	BId1	BId5	BId7	P	S	P	S	P	

NOTE—Component primary (P) and secondary (S) classifications are from Best et al. (2024) and Bardalez Gagliuffi et al. (2015). Combined-light spectral classifications were determined by comparison to spectral standards. S/N groups were assigned based on the 1.20–1.35 μm (J-band) S/N value. For the BId columns, “b” indicates a binary classification and “s” indicates a single classification.

^aBinary identification and confirmation methods: SP = spectral blend binary, V = resolved visual binary, A = astrometric variable, SB1 = radial velocity variable (primary motion).

References— (1) Allers et al. (2010); (2) Allers & Liu (2013); (3) Bardalez Gagliuffi et al. (2014); (4) Bardalez Gagliuffi et al. (2015); (5) Best et al. (2017); (6) Burgasser et al. (2004); (7) Burgasser et al. (2006b); (8) Burgasser et al. (2007a); (9) Burgasser et al. (2008a); (10) Burgasser et al. (2009); (11) Burgasser et al. (2010a); (12) Burgasser et al. (2011b); (13) Burgasser et al. (2011a); (14) Burgasser et al. (2012a); (15) Burgasser et al. (2012b); (16) Burgasser et al. (2015); (17) Chiu et al. (2006); (18) Cruz et al. (2004b); (19) Deacon et al. (2017); (20) Dhital et al. (2011); (21) Dupuy & Liu (2012); (22) Dupuy et al. (2015); (23) Gelino & Burgasser (2010); (24) Gelino et al. (2014); (25) Kellogg et al. (2015); (26) Kirkpatrick et al. (2011); (27) Liu et al. (2012); (28)Looper et al. (2007a); (29) Looper et al. (2007b); (30) Mainzer et al. (2011); (31) Martín et al. (2006); (32) McElwain & Burgasser (2006); (33) Reid et al. (2006b); (34) Sahlmann et al. (2015); (35) Schmidt et al. (2010); (36) Siegler et al. (2007); (37) Burgasser & Splat Development Team (2017).

Of the 43 confirmed binaries with spectra, 25 are identified as binaries by the BId1 model, corresponding to a recall of $R = 0.58$. This performance is considerably poorer than the 0.83–0.89 recall scores from the testing data. To gain insight on this difference, Figure 11 maps the known component types of the binaries, with those identified as a binary by the BId1 model labeled. The binary sample is not uniformly distributed across component type space, with a higher fraction of near equal-component types where all of the RF models show decreased performance (Figure 3). Away from this edge, binary identification is more robust. For the 23 systems with component classifications differing by more than three subtypes, 17 are identified as binary ($R = 0.74$), whereas only 8 of the 20 systems with more similar types are correctly identified ($R = 0.40$).

The BId5 and BId7 models perform even more poorly in aggregate, with sample recall of 0.16 (4/25) and 0.57 (8/14), respectively. These recall values are again far below the 0.76–0.85 and 0.89–0.94 values from our testing sample. The models also have lower recall values compared to the BId1 model (0.60 and 0.79) and the equivalent index-based approaches (0.48 for B14, 0.86 for B10) for the same combined-light spectral ranges. Even if we downselect the binary sample to the primary and secondary classifications encompassed by the B14 ($P \in \{M7, L7\}$, $S \in \{T1, T7\}$) and B10 methods ($P \in \{L5, T2\}$, $S \in \{T2, T7\}$), we obtain only a modest improvement in recall to 0.38 and 0.64 for the BId5 and BId7 models, respectively, whereas the BId1 model (0.88 and 0.82) and indices (0.88 and 1.00) are highly robust in these regimes. Hence, the BId1 model appears to be as good or better than the B10 and B14 indices for binary identification, and far superior to the specialized BId5 and BId7 models.

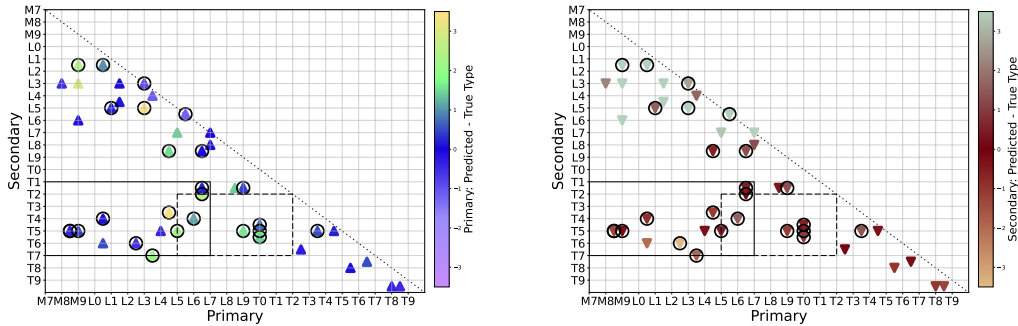


Figure 11. Application of BId1 and BClass1 models for known binaries with SpeX spectral observations (Table 8). The left panel compares primary classifications, the right panel compares secondary classifications. Both panels map individual sources to their reported primary and secondary component types, with those correctly identified as a binary by the BId1 model indicated by large black circles. The color shading indicates the difference between the predicted and reported component types. We also highlight the component type spaces relevant to the B10 (solid line box) and B14 (dashed line box) index classification methods.

For component classification, we quantified recall by requiring that primary and/or secondary types be within 1 subtype (2 subtypes) of the previously published value.

We can see visually in Figure 11 that the majority of primary types are recovered by the BClass1 model with a recall of 0.65 (0.84), secondary types have a lower recall of 0.37 (0.67), and both components are recovered with a recall of 0.23 (0.58). Again, the substandard performance compared to test data can be attributed to the distribution of component classifications in the empirical sample, with misclassifications occurring for systems with similar late-M and L dwarf components (upper left quadrant of Figure 11) and those with large differences between component types (lower left quadrant of Figure 11). For the 23 systems with at least three subtypes separating the primary and secondary component types, and with a T dwarf secondary, there is a modest gain in the accuracy of the secondary classification with a recall of 0.43 (0.70), but primary and combined component recall remains the same. In contrast to our binary identification models, we see clear improvement with the specialized BClass5 and BClass7 models. The BClass5 model outperforms the BClass1 model for primary classification with a recall of 0.76 (0.84), but performs worse for secondary and combined classification recall. For the BClass7 model, if we relax the recall requirement to 2 subtypes, this model performs better in primary classification ($R = 0.86$), secondary classification ($R = 0.93$), and combined classification ($R = 0.79$) for the appropriate combined-light spectral types. Both of these models achieve near-perfect performance if the sample is further downselected to the B10 and B14 component classification ranges.

In summary, the BId1 model appears to perform as well as the B10 and B14 indices, and far better than the specialized RF models BId5 and BId7, in correctly identifying binary spectra, and is particularly robust for systems with differing component classifications (at least three subtypes in this experiment, with 74% of systems recovered). The BClass1 model performs fairly well for primary classification and poorly for secondary classification, whereas the specialized BClass5 and BClass7 models show significantly better performance in their respective spectral type ranges, correctly classifying $\gtrsim 80\%$ of primaries and secondaries to within two subtypes. The lower recall statistics for this sample compared to the synthetic testing data can be explained by the non-uniform composition of real VLM binaries, which are skewed toward early-type and similar-type components.

6. LIMITATIONS OF THE RANDOM FOREST MODEL

Overall, we find our random forest models are superior to current index-based methods for identifying and characterizing very low mass spectral blend binaries in terms of performance, range of applicability, and speed. However, these models also suffer the same inherent limitations in identifying binaries with similar component spectral types or extreme flux ratio systems (e.g., late-M and late-T dwarf pairs). These limitations are relevant for existing binary samples which are dominated by pairs with similar spectral types due to both selection biases (e.g., intrinsically brighter sys-

tems) and the intrinsic prevalence of near-equal mass systems among VLM systems (Burgasser et al. 2003; Fontanive et al. 2018).

Even if we adhere to unbiased, volume-complete samples of very low mass binaries, a relatively small fraction of these systems are suited for detection as spectral blends (Bardalez Gagliuffi et al. 2019b). To illustrate this, we simulated 100,000 VLM binary systems in a volume-limited field sample assuming a uniform age distribution spanning 0.5–8 Gyr, a power-law mass function $\frac{dN}{dM} \propto M^{-0.6}$ for $0.01 M_{\odot} \leq M \leq 0.1 M_{\odot}$ (Kirkpatrick et al. 2024; Best et al. 2024), and a power-law mass ratio distribution $\frac{dN}{dq} \propto q^4$ for $0.2 \leq q \equiv M_2/M_1 \leq 1$ (Burgasser et al. 2003). These simulated systems were evolved to present-day observables using the evolutionary models of Baraffe et al. (2003), and effective temperatures were converted to spectral types using the empirical relation of Pecaut & Mamajek (2013). Figure 12 displays the resulting distribution of component types. A significant fraction of these systems (49%) are mid- and late-T dwarf pairs, consistent with the long-term evolution of brown dwarf systems (Burgasser 2004a; Kirkpatrick et al. 2024), and in a region where binary identification recall drops to $\lesssim 0.5$ (Figure 6). Another 16% of the simulated sample is composed of late-M plus late-M dwarf pairs, primarily stellar-mass systems. Spectral combinations in the B10 or B14 ranges comprise only 8% of the simulated sample. Furthermore, these fractions are consistent to within a few percent over a broad range of assumptions for the mass function and mass ratio distribution. Hence, detectable spectral blend systems generally comprise a small fraction of the overall VLM binary population, as had been previously reported in volume-limited spectral surveys (Bardalez Gagliuffi et al. 2019b).

In addition to poor performance for both near-equal mass and low-temperature very low mass pairs, our random forest models have been trained on a relatively conservative dataset in which peculiar sources (e.g., metal-poor sources, young brown dwarfs, blue L dwarfs) have been excluded. These sources are nevertheless known to be contaminants in spectral blend binary searches (B14). We have also ignored unresolved triple systems, which exist but at low frequencies (Radigan et al. 2013; Sahlmann et al. 2021).

7. SUMMARY AND NEXT STEPS

The key outcomes of this investigation are as follows:

- We have developed a hierarchical set of random forest models that identify unresolved very low mass binary systems from blended light spectra and determine their component spectral types. Our training set was constructed from a sample of late-M, L and T dwarf near-infrared spectra that are used to synthesize both single and blended-light binary spectral templates. For both identification and classification, we tested a series of models to explore performance as a function of spectral signal-to-noise, binary composition, and the inclusion of difference

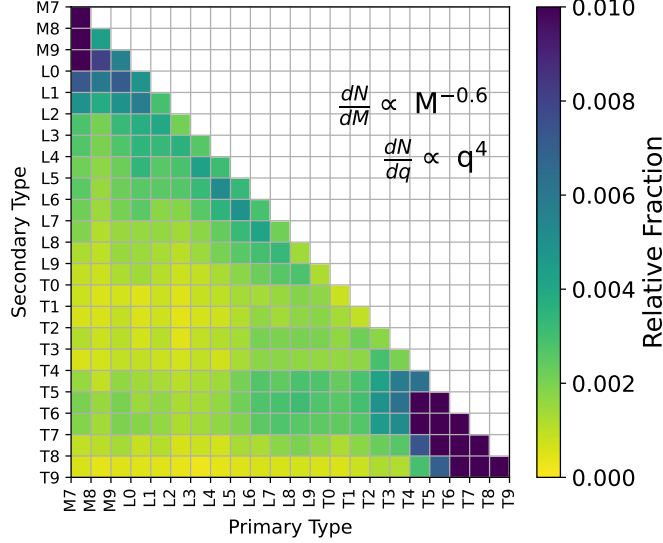


Figure 12. Component spectral type distributions for a simulated sample of VLM dwarf binaries assuming a uniform age distribution over 0.5–8 Gyr, a power-law mass distribution $\frac{dN}{dM} \propto M^{-0.6}$ for $0.01 M_{\odot} \leq M \leq 0.1 M_{\odot}$, a power-law mass ratio distribution $\frac{dN}{dq} \propto q^4$ for $0.2 \leq q \leq 1$, Baraffe et al. (2003) evolutionary models, and the Pecaut & Mamajek (2013) spectral type/effective temperature relation. Color shading indicates the relative density distribution for each spectral type combination.

spectra (after subtracting the best-fit standard spectrum) and masking telluric regions.

- We benchmarked our RF models by assessing the performance of the index-based spectral binary identification methods of B10 and B14, finding these to be poorly suited for general binary combinations (recall = 0.62–0.66 and 0.19–0.27, respectively) but robust (recall $\gtrsim 0.9$) for select component type combinations, specifically L dwarf primaries with T dwarf secondaries.
- Our most reliable RF models for both identification and classification were the most general models, BId1 and BClass1, which are trained on the full spectral range of M6 to T9 dwarfs and their binary combinations. The BId1 identification model achieves a median recall of 0.82–0.89 across the full training set, while the BClass1 classification model yields median errors of $\lesssim 0.1$ subtypes for all components, and systematic uncertainties of ~ 0.5 subtype and ~ 1 subtype for primary and secondary classifications, respectively. Binary identification model variants showed no significant improvement over the BId1 model, while classification models tuned to the B10 and B14 spectral type range improved secondary classification uncertainty to 0.5 subtypes.
- Detailed evaluation of model performance as a function of component spectral type shows that these models are more reliable for certain spectral type combinations, performing optimally for mid-L through mid-T primaries and T dwarf

secondaries, overlapping with the optimal ranges for the B10 and B14 index methods. Classification models are generally robust for primaries across nearly all component types, while secondary classification is generally poor for late-M and L dwarf binaries (similar spectral morphologies) and late-M and mid-/late-T dwarf binaries (large flux differential).

- Feature importance plots indicate that these models are tuned to specific spectral features, notably emission peaks in T dwarf spectra and key VLM spectral absorption features (H_2O , CH_4 , CO bands and K I lines), largely in line with the B10 and B14 spectral index definitions.
- Validation of model performance on the combined-light spectra of known VLM dwarf binary systems indicates decreased performance compared to the training data, driven in large part by the higher frequency of systems with spectral type compositions the RF models are less sensitive too (e.g., M/L dwarf pairs, components with similar spectral types). For sources with larger differences in component types ($\gtrsim 3$ subtypes), the BId1 binary identification model achieves robust performance (recall > 0.8), comparable to or better than index-based methods. For classification, the BClass5 model (matched to the B14 index method) and the BClass7 model (matched to the B10 index method) have better performance, with robust recall of primary and secondary classifications to within 2 subtypes.
- The primary strength of the RF models is their speed, with training times measured in seconds and identification and classification of individual spectra measured in milliseconds on a typical laptop computer. On the other hand, these models have the same limitations inherent to the spectral blend method, namely low sensitivity to systems with similar component spectral types and those with extreme flux ratios. These limitations imply that only a small fraction ($\sim 8\%$) of VLM binaries in a field population are likely to be identified by this approach.

There are a number of ways that the machine learning approach described here can be improved for very low mass binary studies. Expansion of the breadth of spectral data included in the modeling could improve performance for both identification and classification. Optical spectral data are more sensitive to the primary components of VLM binaries, while mid-infrared data improves the detection and characterization of low-temperature T dwarf companions (cf. [Burgasser et al. 2008c](#)). The flexibility of RF models also enables the use of non-spectral data as features. For example, VLM dwarfs with known distances through parallax measurement, cluster membership, or association with co-moving companion could make use of absolute flux measurements to improve the detection of systems with similar masses and spectral types. The training data used for these models can be also adjusted to more accurately reflect the underlying mass ratio, age distribution, and stellar/substellar evolution of the VLM population being studied, rather than equal distributions across spectral type

pairs (Figure 12). Moreover, while the specialized RF models tailored for the B10 and B14 index-based methods improved performance only for component classification, the speed of model training (seconds) suggests that individualized RF models could be constructed for specific combined-light or component spectral type groups; e.g., focusing on equal or extreme light-ratio systems. Finally, our exploration of the binary identification and classification problem focused only on random forest models. Alternate ML architectures, such as support vector machines or neural networks, may be better suited for this task given the high dimensionality of data, particularly if non-spectral data are included (Baron 2019).

A natural next step is to apply the machine learning framework explored in this study to additional spectral survey samples to search for new binaries. Beyond the SpeX prism sample investigated here, there are growing libraries of VLM infrared spectra obtained with space-based platforms such as JWST (Beiler et al. 2024; Luhman et al. 2024; Tu et al. 2025; Morrissey et al. 2025) and Euclid (Žerjal et al. 2025; Mohandasan et al. 2025; Dominguez-Tagle et al. 2025), and future samples that are expected from SPHEREx (Doré et al. 2014) and the Nancy Grace Roman Space Telescope (Mosby et al. 2020). For these datasets, similar models could be deployed with the appropriate empirical or synthetic training sets. Our initial study demonstrates that these approaches can address both potential biases and bottlenecks in the identification of VLM binary systems for population studies.

ACKNOWLEDGMENTS

JDDG and MD acknowledge funding from the UCSD Summer Undergraduate Research Program. This work has benefited from The UltracoolSheet at <http://bit.ly/UltracoolSheet>, maintained by Will Best, Trent Dupuy, Michael Liu, Aniket Sanghi, Rob Siverd, and Zhoujian Zhang. We also thank our anonymous referee for their comments which improved the quality of this manuscript. Data presented in this paper were obtained with the NASA Infrared Telescope Facility (IRTF) on the summit of Maunakea. Spectral template data is available on Zenodo under an open-source Creative Commons Attribution license for SPLAT v1.11: [doi:10.5281/zenodo.17107529](https://doi.org/10.5281/zenodo.17107529). The authors recognize and acknowledge the significant cultural role and reverence that the summit of Maunakea has with the indigenous Hawaiian community, and that IRTF stands on Crown and Government Lands that the State of Hawai'i is obligated to protect and preserve for future generations of indigenous Hawaiians. Portions of this work were conducted at the University of California, San Diego, which was built on the unceded territory of the Kumeyaay Nation, whose people continue to maintain their political sovereignty and cultural traditions as vital members of the San Diego community.

Facilities: IRTF(SpeX)

Software: astropy (Astropy Collaboration et al. 2013, 2018, 2022), Matplotlib (Hunter 2007), NumPy (Harris et al. 2020), pandas (McKinney et al. 2010), scikitlearn (Pedregosa et al. 2011), SPLAT (Burgasser & Splat Development Team 2017),

APPENDIX

The training sample used in this work was constructed from low-resolution near-infrared spectra of late-M, L, and T dwarfs contained in the SpeX Prism Library Analysis Toolkit (SPLAT [Burgasser & Splat Development Team 2017](#)), and obtained with the SpeX spectrograph on the NASA 3m Infrared Telescope Facility ([Rayner et al. 2003](#)) using its low-resolution prism-dispersed mode. Table 9 lists the 1006 spectra used in this study. in order of increasing spectral type and S/N. Classifications are based on the best χ^2 match to near-infrared spectral standards defined in [Kirkpatrick et al. \(2010, M and L dwarfs\)](#) and [Burgasser et al. \(2006b, T dwarfs\)](#). S/N values were measured in the 1.2–1.35 μm *J*-band region and assigned to low ($2 \leq \text{S/N} < 50$), med ($50 \leq \text{S/N} < 100$), and high ($\text{S/N} \geq 100$) S/N groups. References are given for the original data publication. All of the original spectra can be accessed from the SPLAT archive v1.11¹² ([Burgasser et al. 2025](#)), and we have made the specific training set for our models available on Zenodo at [doi: 10.5281/zenodo.15611798](https://doi.org/10.5281/zenodo.15611798).

Table 9. SpeX Spectral Sample.

SIMBAD Name	SpT	S/N	S/N Class	Ref
2MASS J01141304+4354287	M6	41	low	40
2MASS J20033545+1158552	M6	45	low	42
LEHPM 2–1973	M6	61	mid	3
2MASS J00583814–1747311	M6	73	mid	8
2MASS J18244344+2937133	M6	75	mid	8
2MASS J01532750+3631482	M6	93	mid	8
2MASS J01405263+0453302	M6	94	mid	42
LHS 3566	M6	98	mid	8
2MASS J11304030+1206306	M6	101	high	42
2MASS J22465014–0643357	M6	109	high	8
2MASS J04555288+3006523	M6	119	high	59
2MASS J16062870–2856580	M6	144	high	24
2MASS J15501958–2805237	M6	149	high	24
2MASS J15544486–2843078	M6	175	high	24
2MASSI J1441045+271932	M6	191	high	3
2MASS J11073750–2759385B	M6	196	high	3
Wolf 359	M6	206	high	16
2MASS J04314644+2506236	M6	214	high	55
2MASS J04102834+2051507	M6	218	high	29
LHS 1375	M6	222	high	42
2MASS J15572692–2715094	M6	222	high	24
2MASS J15490803–2839550	M6	241	high	24
2MASS J15524857–2621453	M6	249	high	24
2MASS J15493660–2815141	M6	260	high	24

Table 9 continued on next page¹² <https://github.com/aburgasser/splat>

Table 9 (*continued*)

SIMBAD Name	SpT	S/N	S/N Class	Ref
2MASS J16002535–2644060	M6	291	high	24
2MASS J15491602–2547146	M6	343	high	24
2MASS J15492909–2815384	M6	397	high	24
GJ 3693	M6	427	high	3
LHS 2090	M6	601	high	3
GJ 1111	M6	856	high	3
SDSS J07351959+4108503	M7	26	low	3
2MASS J17330480+0041270	M7	40	low	8
2MASS J23270985+2341364	M7	42	low	8
2MASS J14171672–0407311	M7	45	low	8
2MASS J15243203+0934386	M7	45	low	8
2MASS J11070582+2827226	M7	52	mid	8
2MASS J12121714–2253451	M7	56	mid	8
WISE J141144.14–140301.1	M7	59	mid	70
2MASS J15561873+1300527	M7	59	mid	8
2MASS J04035944+1520502	M7	60	mid	8
SDSS J12455566+4902109	M7	64	mid	3
2MASS J13593574+3031039	M7	66	mid	8
2MASS J16403197+1231068	M7	68	mid	8
2MASS J09171104–1650010	M7	69	mid	42
2MASS J04400067+2358211	M7	69	mid	49
WISE J01163905–1654205	M7	73	mid	66
2MASS J03382862+0001296	M7	73	mid	42
2MASS J00412179+3547133	M7	73	mid	8
2MASS J12341814+0008359	M7	75	mid	42
2MASS J15412408+5425598	M7	76	mid	8
2MASS J01151621+3130061	M7	80	mid	8
SDSS J15525232–0035019	M7	93	mid	3
LSPM J2331+4607N	M7	94	mid	3
2MASS J04071296+1710474	M7	97	mid	8
2MASS J00335534–0908247	M7	99	mid	8
WISE J144127.49–515807.6	M7	103	high	70
2MASS J18355309–3217129	M7	105	high	42
2MASS J17561080+2815238	M7	106	high	42
2MASS J00115060–1523450	M7	107	high	8
2MASS J16210822+2938480	M7	111	high	3
2MASS J04584239–3002061	M7	135	high	33
WISE J194128.98–342335.8	M7	137	high	53
WISE J235408.36+551854.5	M7	139	high	53
2MASS J18284076+1229207	M7	151	high	42
2MASS J14343616+2202463	M7	162	high	68
WISE J030601.64–033058.4	M7	170	high	44
WISE J08522436+5139255	M7	171	high	44
SDSS J075054.74+445418.7	M7	171	high	70
SDSS J010637.33+151855	M7	180	high	43
LSR 1826+3014	M7	183	high	8
SDSS J03083243–08105138	M7	202	high	3

Table 9 *continued on next page*

Table 9 (*continued*)

SIMBAD Name	SpT	S/N	S/N Class	Ref
WISE J033713.43+114824.6	M7	207	high	70
GRH 2208–2007	M7	209	high	3
SSSPM J2400–2008	M7	225	high	3
WISE J10230404+1556164	M7	268	high	44
LEHPM 2–461	M7	269	high	3
LHS 523	M7	289	high	3
SDSS J093128.22+052821.93	M7	323	high	3
2MASS J09524622+0620410	M7	325	high	3
2MASS J08490052+0220155	M7	341	high	3
SDSS J16311227+32271141	M7	343	high	3
SDSS J090206.90+003319.36	M7	348	high	3
GJ 660.1B	M7	348	high	1
LHS 2351	M7	364	high	3
GAT 1370	M7	381	high	16
2MASS J04485745+2913521	M7	454	high	29
2MASS J04251550+2829275	M7	461	high	55
LP 775–31	M7	528	high	3
VB 8	M7	608	high	16
SDSS J204724.7+142152	M8	11	low	3
2MASS J00100480–0930519	M8	24	low	40
2MASS J09264992+5230435	M8	27	low	34
2MASS J22582325+2906484	M8	29	low	40
HD 114762B	M8	33	low	6
SIMP J01031050+1940463	M8	38	low	62
2MASS J23363834+4523306	M8	40	low	8
2MASS J16592987+2055298	M8	42	low	39
2MASS J01194279+1122427	M8	47	low	40
2MASS J03440599+3215321	M8	47	low	54
2MASS J04230607+2801194	M8	48	low	49
2MASS J05341594–0631397	M8	48	low	42
SIMP J03574959–1937538	M8	55	mid	62
SIMP J21430506–1544394	M8	56	mid	62
2MASS J20494090+1140068	M8	56	mid	8
2MASS J10454932+1254541	M8	57	mid	42
SIMP J22030176–0301107	M8	59	mid	62
2MASS J09243114+2143536	M8	63	mid	42
2MASS J14442946+0048530	M8	65	mid	3
2MASS J23335838+0050110	M8	66	mid	3
WISE J232219.45–140726.2	M8	67	mid	53
SDSS J07342570+30065792	M8	67	mid	3
2MASS J16390818+2839015	M8	68	mid	71
2MASS J04290068+2755033	M8	68	mid	55
SDSS J13331279+1509566	M8	69	mid	3
2MASS J00082822+3125581	M8	69	mid	40
2MASS J13342806+5258199	M8	71	mid	42
2MASS J13080147+3553169	M8	72	mid	42
WISE J000131.93–084126.9	M8	73	mid	53

Table 9 *continued on next page*

Table 9 (*continued*)

SIMBAD Name	SpT	S/N	S/N Class	Ref
SDSS J233350.76-000011.3	M8	74	mid	3
SIMP J01481626+3712421	M8	74	mid	62
2MASS J04242090+2630511	M8	76	mid	55
2MASS J01470204+2120242	M8	76	mid	8
2MASS J23092857+3246175	M8	78	mid	42
2MASS J12321827-0951502	M8	81	mid	3
2MASS J15201746-1755307	M8	82	mid	42
2MASS J11150577+2520467	M8	83	mid	8
2MASS J21100889+2132483	M8	84	mid	8
2MASS J01335299+0033017	M8	85	mid	3
2MASS J23343177-1509294	M8	87	mid	42
2MASS J17364839+0220426	M8	89	mid	8
2MASS J16443963+2600128	M8	92	mid	62
2MASS J22021302-0228558	M8	96	mid	42
SDSS J08354533+2224308	M8	98	mid	3
2MASS J15141384+1201451	M8	100	mid	42
SDSS J234654.7-315353	M8	101	high	3
ULAS J22585405+0113512	M8	102	high	3
WISE J030845.36+325923.1	M8	104	high	53
2MASS J00552554+4130184	M8	105	high	8
2MASS J01330461-1355271	M8	105	high	42
2MASS J00163761+3448368	M8	105	high	42
WISE J222409.64-185242.1	M8	106	high	53
2MASSI J0032431-223727	M8	107	high	3
2MASS J21050130-0533505	M8	108	high	39
2MASS J08315564+1025466	M8	110	high	3
2MASS J04325119+1730092	M8	113	high	51
2MASS J04340619+2418508	M8	116	high	55
2MASSI J1717045+150953	M8	117	high	3
SIMP J16275003+0836036	M8	117	high	62
SDSS J215339.77+295005	M8	119	high	3
DENIS J104617.0-421237	M8	121	high	3
2MASS J09384022-2748184	M8	121	high	42
SDSS J231725.15-005433.6	M8	123	high	3
HB 2126-4459	M8	123	high	3
SDSS J00220934-0110397	M8	129	high	3
SDSS J14205830+2131566	M8	130	high	3
2MASS J15551960-2751207	M8	131	high	24
WISE J09165718-1121047	M8	134	high	44
2MASS J19561542-1754252	M8	138	high	3
2MASS J14313097+1436539	M8	141	high	68
WISE J083450.79+642526.1	M8	143	high	70
SDSS J17104934+33232518	M8	144	high	3
SDSS J17254384+5325349	M8	144	high	3
SDSS J13571490-1438520	M8	149	high	3
2MASS J12531161+2728145	M8	151	high	68
SDSS J230809.9-313122	M8	152	high	3

Table 9 *continued on next page*

Table 9 (*continued*)

SIMBAD Name	SpT	S/N	S/N Class	Ref
SDSS J11491231-0153006	M8	152	high	3
SDSS J14525558+2723244	M8	152	high	3
SDSS J17175402+64274503	M8	155	high	3
SDSS J233224.38-005025	M8	155	high	3
SDSS J213307.94+232159	M8	156	high	3
2MASS J05363713-0328492	M8	157	high	42
2MASS J22225588-4446197	M8	161	high	42
2MASS J20575592-0050060	M8	165	high	3
2MASS J2306292-050227	M8	165	high	35
WISE J100926.40+354137.5	M8	166	high	70
DENIS J0427270-112713	M8	168	high	3
LEHPM 1-3396	M8	168	high	3
SSSPM J2356-3426	M8	170	high	3
SDSS J232313.4-024435	M8	171	high	3
HB 2124-4228	M8	171	high	3
SDSS J212033.89+102159	M8	172	high	3
DENIS JJ1934511-184134	M8	176	high	3
HB 2115-4518	M8	184	high	3
2MASS J21233110-2345180	M8	185	high	3
LEHPM 2153	M8	191	high	3
2MASS 04441479+0543573	M8	195	high	3
2MASS J0407089-234829	M8	200	high	3
2MASS J01145788+4318561	M8	200	high	40
SDSS J081946.02+165853.9	M8	201	high	3
2MASS J03201710-1026120	M8	203	high	3
2MASS J15573270+1752380	M8	204	high	3
SDSS J183929.17+442438	M8	204	high	3
2MASPJ2234330+291850	M8	204	high	3
2MASS J04081032+0742494	M8	204	high	3
SDSS J010311.51-004417	M8	209	high	3
LP 944-20	M8	209	high	16
VB 10	M8	210	high	8
SDSS J214956.55+060334	M8	215	high	3
LEHPM 2-287	M8	217	high	3
SIPS J0050-1538	M8	217	high	3
2MASS J03442156+3215098	M8	219	high	54
DENIS J02065660-0735190	M8	220	high	3
2MASS J07140394+3702459	M8	224	high	33
2MASS 10213232-2044069	M8	226	high	3
2MASS J03320043-2317496	M8	226	high	3
DENIS J1019245-270717	M8	227	high	3
WISE J174336.62+154901.3	M8	233	high	53
2MASS J17281134+0839590	M8	237	high	3
2MASS J08391608+1253543	M8	237	high	3
2MASS J12373441+3028596	M8	239	high	68
2MASS J14122270+2354100	M8	241	high	3
LEHPM 2-471	M8	244	high	3

Table 9 continued on next page

Table 9 (*continued*)

SIMBAD Name	SpT	S/N	S/N Class	Ref
2MASS J14351087-2333025	M8	245	high	52
2MASS J04440164+1621324	M8	246	high	29
2MASS J00100009-2031122	M8	246	high	3
SDSS J16351918+42230531	M8	247	high	3
SDSS J084403.46+043436.19	M8	247	high	3
2MASS J03354535+0658058	M8	252	high	3
LEHPM 2-381	M8	253	high	3
2MASS J13595510-4034582	M8	257	high	3
2MASS 09474477+0224327	M8	259	high	3
SDSS J23371664-09332480	M8	260	high	3
SSSPM J0124-4240	M8	260	high	3
2MASS J2341286-113335	M8	262	high	3
2MASS J03350208+2342356	M8	269	high	2
LEHPM 2-498	M8	270	high	3
2MASS J16082460+195747	M8	278	high	3
2MASS J2035203-311008	M8	279	high	3
2MASS J04264449+2756433	M8	279	high	55
2MASS J19233810-3308410	M8	290	high	3
LP 655-23B	M8	296	high	3
2MASS J08352366+1029318	M8	296	high	3
2MASS J09161504+2139512	M8	297	high	3
2MASS J16090168-2740521	M8	301	high	24
2MASS J01170586+1752568	M8	305	high	42
2MASS J11240487+3808054	M8	308	high	8
2MASS J0007078-245804	M8	311	high	3
LEHPM 1-606	M8	312	high	3
2MASS J21263403-3143220	M8	318	high	3
LHS 2195	M8	319	high	3
2MASS J15345700-1418480	M8	320	high	3
SDSS J01071600-1517570	M8	324	high	3
2MASS J16490419+0444571	M8	328	high	3
SDSS J02540582-1934523	M8	329	high	3
2MASS J20491972-1944324	M8	334	high	8
LEHPM 1-6443	M8	336	high	16
LEHPM 2-50	M8	337	high	3
SDSS J105547.29+080842.64	M8	337	high	3
LEHPM 1-162	M8	337	high	3
DENIS-P J2353-0833	M8	339	high	3
LHS 3003	M8	353	high	3
2MASS J03305571+3146272	M8	358	high	42
SDSS J100319.17-010508.15	M8	362	high	3
LEHPM 2-333	M8	363	high	3
SDSS J02511323+00473631	M8	363	high	3
2MASS J00085931+2911521	M8	365	high	71
LEHPM 1-6333	M8	372	high	16
2MASS J00550460-3052000	M8	386	high	3
LEHPM 1-3070	M8	406	high	3

Table 9 *continued on next page*

Table 9 (*continued*)

SIMBAD Name	SpT	S/N	S/N Class	Ref
LEHPM 2–436	M8	407	high	3
2MASS J2352050–110043	M8	416	high	3
2MASS J03540135+2316330	M8	427	high	3
LP 851–346	M8	430	high	3
LHS 2243	M8	443	high	3
LHS 132	M8	466	high	3
2MASS J03395284+2457270	M8	492	high	3
2MASS J05441150–2433010	M8	499	high	3
SDSS J04270723+0859027	M8	507	high	3
2MASS J08303256+0947150	M8	612	high	3
LHS 2034	M8	640	high	3
LHS 1604	M8	1063	high	3
SIMP J04144834+1529007	M9	43	low	62
2MASS J09194512+5135149	M9	45	low	40
2MASS J21403907+3655563	M9	46	low	42
2MASS J16470847+5120088	M9	49	low	39
SDSS J09323747+6725145	M9	65	mid	3
2MASS J05314149+6856293	M9	67	mid	42
2MASS J14185890+6000194	M9	70	mid	42
2MASS J17033593+2119071	M9	71	mid	42
2MASS J00451330+1228538	M9	71	mid	42
2MASS J23443744–0855075	M9	71	mid	39
2MASS J01574939–1146113	M9	73	mid	42
SDSS J001637.62–103911.2	M9	74	mid	3
2MASS J21483083+0020540	M9	76	mid	3
SDSS J09385888+0443439	M9	83	mid	3
SDSS J232136.11–002819.1	M9	84	mid	3
SDSS J01084048+1347392	M9	90	mid	3
2MASS J13120700+3937440	M9	94	mid	3
2MASS J22044198–0036510	M9	98	mid	3
2MASS J23531922+3656457	M9	101	high	42
2MASS J12425052+2357231	M9	101	high	42
2MASS J22355013+1227370	M9	105	high	3
2MASS J14403186–1303263	M9	106	high	42
DENIS J124744.2–381646	M9	107	high	32
2MASS J01165457–1357342	M9	108	high	3
SDSS J225003.72+143046.7	M9	112	high	3
2MASS J13373116+4938367	M9	120	high	3
SDSS J08362199+4949315	M9	121	high	3
SDSS J09413492+1009421	M9	127	high	3
SDSS J153012.87+514717.1	M9	131	high	71
SDSSp J163600.79–003452.6	M9	140	high	3
SDSS J01535423+1404528	M9	144	high	3
2MASS J01460119–4545263	M9	145	high	3
2MASS J15004572+4219448	M9	146	high	3
SDSS J213435.61+240408	M9	151	high	3
2MASS J21472764+0101040	M9	152	high	34

Table 9 *continued on next page*

Table 9 (*continued*)

SIMBAD Name	SpT	S/N	S/N Class	Ref
SDSS J15102955+36194699	M9	154	high	3
2MASS J0417474-212919	M9	161	high	3
SDSS J08264265+19392195	M9	181	high	3
2MASS J01273917+2805536	M9	184	high	3
2MASS J17343053-1151388	M9	202	high	42
G 225-36B	M9	214	high	70
2MASS J18064570+2923591	M9	215	high	3
2MASS J05170548-4154413	M9	230	high	3
2MASS J0355201+143929	M9	243	high	3
2MASS J15485834-1636018	M9	249	high	3
2MASS J0534584-151143	M9	252	high	3
2MASS J0000286-124515	M9	259	high	3
2MASS J10220489+0200477	M9	261	high	3
LEHPM 2-183	M9	271	high	3
PSS 1458+2839	M9	278	high	3
2MASS J23294790-1607550	M9	283	high	42
2MASS J03521086+0210479	M9	344	high	3
BRI 1222-1222	M9	372	high	3
2MASS J03264453+1919309	M9	404	high	3
LHS 2924	M9	440	high	11
2MASS J08594029+1145325	M9	498	high	3
2MASS J13170488+3447513	L0	27	low	40
2MASS J04510592+0014394	L0	35	low	40
2MASS J15525579+1123523	L0	38	low	40
2MASS J22545900-0330590	L0	41	low	40
SIMP J15014711-1831272	L0	50	mid	62
2MASS J21115335-0644172	L0	57	mid	39
SDSS J17031670+19063603	L0	67	mid	3
DENIS-P J0020.9-4414	L0	70	mid	3
2MASS J01205253+1518277	L0	71	mid	62
SDSS J10330910+1216259	L0	76	mid	3
2MASS J00265329-0936267	L0	82	mid	62
2MASS J21111559-0543437	L0	83	mid	39
SDSS J14060148+5249309	L0	84	mid	3
SDSSp J225529.09-003433.4	L0	87	mid	3
DENIS-P J1047-1815	L0	88	mid	2
2MASSI J1707333+430130	L0	90	mid	3
SDSS J000632.60+140606.4	L0	90	mid	3
2MASS J03442997+3219227	L0	91	mid	54
2MASS J16242936+1251451	L0	92	mid	39
PC 0025+04	L0	94	mid	2
2MASS J12490872+4157286	L0	95	mid	42
SDSS J08364634+0526426	L0	99	mid	3
SDSS J10340567+0350163	L0	105	high	3
SDSS J074756.31+394732.9	L0	107	high	3
2MASS J14022235+0648479	L0	108	high	3
SDSS J00570556-0846241	L0	109	high	3

Table 9 *continued on next page*

Table 9 (*continued*)

SIMBAD Name	SpT	S/N	S/N Class	Ref
2MASS J23312935+1552220	L0	139	high	3
2MASSW J1300425+191235	L0	142	high	3
2MASSI J0239424-173547	L0	147	high	3
SDSS J03440891+0111249	L0	158	high	3
DENIS-P J1157480-484442	L0	172	high	3
2MASS J20263647+0439400	L0	177	high	3
SDSS J23352642+0817213	L0	178	high	3
2MASS J08041429+0330474	L0	181	high	3
2MASSI J0502134+144236	L0	196	high	3
2MASS J08593854+6341355	L0	200	high	3
DENIS-P J1733423-165449	L0	221	high	3
2MASSW 1421314+182740	L0	224	high	3
2MASS J16184503-1321297	L0	228	high	3
2MASS J23453903+0055137	L0	230	high	3
2MASSI J2254519-284025	L0	235	high	3
2MASS J08533434-0329432	L0	237	high	3
2MASS J09352803-2934596	L0	250	high	3
2MASS J02594471+2254443	L0	290	high	3
DENIS-P J0652197-253450	L0	292	high	3
SDSS J044337.61+000205.1	L0	305	high	3
WISE J19064847+4011068	L0	332	high	37
2MASS J15101685-024107	L0	333	high	3
TVLM 513-46546	L0	357	high	3
2MASS J22341394+2359559	L0	360	high	8
2MASS J02284243+1639329	L0	379	high	3
2MASS J17312974+2721233	L0	533	high	2
2MASS J2320292+412341	L1	32	low	3
2MASS J14124574+3403074	L1	33	low	40
2MASS J22035781+0713492	L1	40	low	40
WISE J134310.44-121628.8	L1	40	low	53
2MASS J15163838+3333576	L1	41	low	40
2MASS J01001471-0301494	L1	45	low	40
2MASS J11282763+5934003	L1	46	low	40
2MASS J16360752+2336011	L1	48	low	39
WISE J124135.43-245748.8	L1	50	mid	45
SIMP J22484809-0126570	L1	50	mid	62
2MASSI J0104075-005328	L1	51	mid	3
WISE J211807.07-321713.5	L1	55	mid	53
2MASS J04223057+0723448	L1	57	mid	62
SIMP J18115567+2728407	L1	58	mid	62
2MASS J14232186+6154005	L1	58	mid	34
SDSS J062621.22+002934.2	L1	59	mid	3
2MASS J01343635-0145444	L1	64	mid	40
SDSS J211846.77-001044.6	L1	64	mid	3
WISE J195113.62-331115.7	L1	66	mid	70
SDSS J143933.44+031759.2	L1	69	mid	3
SDSS J214046.55+011259.7	L1	71	mid	3

Table 9 continued on next page

Table 9 (*continued*)

SIMBAD Name	SpT	S/N	S/N Class	Ref
2MASS J09481259+5300387	L1	73	mid	40
2MASSI J2054358+151904	L1	73	mid	3
2MASS J17320014+2656228	L1	73	mid	42
2MASS J13384944+0437315	L1	74	mid	3
2MASS J15433947-2535549	L1	75	mid	24
2MASS J13083106+0818522	L1	77	mid	62
2MASS J04102390+1459104	L1	77	mid	62
2MASS J02301551+2704061	L1	78	mid	42
2MASSI J2057153+171515	L1	80	mid	3
SDSS J08181228+3310482	L1	80	mid	3
2MASSW J0242435+160739	L1	81	mid	3
2MASSW J1338261+414034	L1	83	mid	3
WISE J052857.68+090104.4	L1	84	mid	70
SDSS J10174251+4310579	L1	84	mid	3
2MASS J16301770-2120010	L1	85	mid	3
SDSS J165329.69+623136.5	L1	86	mid	19
2MASS J14520183+1114590	L1	87	mid	3
SSSPM J0219-1939	L1	88	mid	3
2MASS J01340281+0508125	L1	88	mid	42
DENIS J21391360-3529500	L1	91	mid	3
SIPS J0614-2019	L1	91	mid	3
SDSS J08175749+1824050	L1	92	mid	3
2MASS J13313310+3407583	L1	93	mid	42
2MASS J01472702+4731142	L1	93	mid	42
SDSS J214527.82-073434.2	L1	94	mid	3
SDSS J11264703+5816322	L1	95	mid	3
SDSS J10515124+13111633	L1	97	mid	3
SDSS J172244.32+632946.8	L1	97	mid	3
SDSS J161611.36+521328	L1	98	mid	71
2MASS J00285545-1927165	L1	102	high	3
SDSS J08410685+6035063	L1	102	high	3
2MASS J12073804-3909050	L1	104	high	3
DENIS J1206501-393725	L1	105	high	3
2MASS J07415784+0531568	L1	105	high	42
HD 91702B	L1	106	high	62
SDSS J035308.54+103056	L1	106	high	3
DENIS-P J1323-1806	L1	107	high	3
SDSS J004154.54+134135.5	L1	110	high	3
DENIS J1707252-013809	L1	111	high	3
BRLT 317	L1	111	high	62
2MASS J08270185+4129191	L1	114	high	40
SDSS J003843.99+134339.5	L1	117	high	3
SIMP J22543828+1640488	L1	117	high	62
2MASS J06050190-2342260	L1	117	high	3
2MASS J05264348-4455455	L1	118	high	3
SDSS J16545079+3747146	L1	119	high	3
SDSS J080048.13+465825.5	L1	119	high	3

Table 9 *continued on next page*

Table 9 (*continued*)

SIMBAD Name	SpT	S/N	S/N Class	Ref
SDSS J09094813+1940439	L1	121	high	3
DENIS J02304500-0953050	L1	122	high	3
SDSSp J005406.55-003101.8	L1	123	high	3
SDSS J16585026+1820006	L1	125	high	3
2MASS J13061727+3820296	L1	127	high	3
2MASSI J1807159+501531	L1	128	high	16
SDSS J15564435+1723089	L1	128	high	3
SDSS J14324210+3451427	L1	129	high	3
DENIS J20131080-1242440	L1	129	high	3
SDSS J13334536-0216002	L1	129	high	3
2MASS J05301261+6253254	L1	129	high	3
SDSS J104842.84+011158.5	L1	133	high	16
2MASS J20343769+0827009	L1	133	high	19
2MASS J08355829+0548308	L1	134	high	3
SDSS J023547.56-084919.8	L1	136	high	3
2MASS J10511900+5613086	L1	137	high	3
2MASS J15230657-2347526	L1	137	high	3
SDSS J14225715+0827521	L1	137	high	3
SDSS J001911.65+003017.8	L1	142	high	3
2MASSW J1035245+250745	L1	143	high	3
SIPS J0031-3840	L1	143	high	3
2MASS J00320509+0219017	L1	144	high	3
SDSS J08583697+2710508	L1	144	high	3
2MASS J00145575-4844171	L1	144	high	41
2MASSW J0147334+345311	L1	146	high	3
SDSS J08433328+1024435	L1	148	high	3
WISE J062442.37+662625.6	L1	150	high	20
G 203-50B	L1	151	high	3
2MASSW J0228110+253738	L1	156	high	16
2MASS J14090310-3357565	L1	165	high	3
2MASS J14044495+4634297	L1	166	high	3
SSSPM J2310-1759	L1	167	high	3
2MASS J20135152-2806020	L1	177	high	2
2MASS J13015465-1510223	L1	177	high	3
HD 149361B	L1	177	high	3
2MASS J04012977-4050448	L1	177	high	3
2MASS J09211410-2104446	L1	177	high	14
LEHPM 1-494B	L1	182	high	3
2MASSI J0408290-145033	L1	184	high	3
2MASS J13364062+3743230	L1	185	high	3
WISE J07155238-1145329	L1	189	high	44
SDSS J161928.31+005011.9	L1	191	high	3
DENIS J2308113-272200	L1	195	high	3
2MASS J23211254-1326282	L1	195	high	3
2MASSI J2107316-030733	L1	197	high	8
2MASS J00464841+0715177	L1	198	high	3
2MASS J21371044+1450475	L1	199	high	3

Table 9 *continued on next page*

Table 9 (*continued*)

SIMBAD Name	SpT	S/N	S/N Class	Ref
2MASS J23302258-0347189	L1	199	high	3
2MASS J11533966+5032092	L1	202	high	3
DENIS J23545990-1852210	L1	202	high	3
2MASS J16573454+1054233	L1	206	high	3
2MASSW J2130446-084520	L1	206	high	3
2MASSW J1412244+163312	L1	208	high	3
2MASSW J0058425-065123	L1	211	high	3
DENIS-P J1745346-164053	L1	211	high	3
2MASS J19355595-2846343	L1	214	high	2
DY Psc	L1	215	high	3
DENIS-P J153941.96-052042.4	L1	216	high	3
2MASS J16134550+1708270	L1	217	high	3
HD 89744B	L1	218	high	16
DENIS-P J0716478-063037	L1	219	high	3
WISE J162359.70-050811.4	L1	226	high	70
2MASS J06411840-4322329	L1	228	high	3
2MASSI J1721039+334415	L1	228	high	3
2MASS J12212770+0257198	L1	240	high	16
2MASSI J1204303+321259	L1	243	high	3
DENIS-P J1159+0057	L1	245	high	3
2MASSW J0832045-012835	L1	252	high	3
DENIS-P J170548.38-051645.7	L1	256	high	19
SDSS J232246.84-313323	L1	256	high	3
2MASS J01490895+2956131	L1	264	high	3
2MASSW J1018588-290953	L1	264	high	3
DENIS-P J0909-0658	L1	265	high	3
2MASSW J1645221-131951	L1	272	high	16
2MASSI J0451009-340214	L1	291	high	3
SDSS J14380829+64083631	L1	297	high	3
SDSS J09230870+2340137	L1	302	high	3
2MASSW J1555157-095605	L1	306	high	3
2MASSI J2057540-025230	L1	327	high	8
2MASS J10224821+5825453	L1	327	high	3
DENIS-P J0615493-010041	L1	341	high	3
2MASSW J1155395-372735	L1	351	high	3
DENIS-P J0751164-253043	L1	355	high	3
2MASS J09532126-1014205	L1	373	high	3
SSSPM 0829-1309	L1	416	high	14
2MASSI J0428510-225323	L1	418	high	3
2MASSW J1439284+192915	L1	442	high	8
LSR 0602+3910	L1	465	high	3
2MASS J03140344+1603056	L1	583	high	3
2MASS J10551343+2504028	L2	25	low	40
2MASS J14154242+2635040	L2	30	low	40
2MASS J23053808+0524070	L2	35	low	40
2MASS J22114470+6856262	L2	35	low	3
2MASS J12492272+0310255	L2	40	low	40

Table 9 *continued on next page*

Table 9 (*continued*)

SIMBAD Name	SpT	S/N	S/N Class	Ref
2MASS J17570962+4325139	L2	40	low	40
2MASS J02151451+0453179	L2	41	low	40
WISE J212354.78−365223.4	L2	47	low	53
SDSS J08475148+0138110	L2	48	low	3
2MASS J00435012+0928429	L2	49	low	40
2MASS J09083688+5526401	L2	50	mid	40
SIMP J13174922+0448149	L2	51	mid	62
2MASS J04335245+2612548	L2	51	mid	49
2MASSI J2104149−103736	L2	57	mid	19
WISE J06074213+4550370	L2	59	mid	44
2MASS J00501771+1012528	L2	59	mid	40
2MASS J10315064+3349595	L2	60	mid	42
2MASS J13081228+6103486	L2	63	mid	34
2MASS J21075409−4544064	L2	63	mid	3
2MASS J22295358+1556180	L2	69	mid	40
SDSS J225913.88−005158.2	L2	71	mid	3
WISE J13482442−4227449	L2	77	mid	45
2MASS J16091145+2116587	L2	78	mid	39
SIMP J04323767−0639501	L2	81	mid	62
2MASS J14182962−3538060	L2	81	mid	42
2MASSI J0753321+291711	L2	83	mid	3
2MASS J21555848+2345307	L2	83	mid	42
2MASSI J0224367+253704	L2	83	mid	3
SDSS J08430794+3141292	L2	85	mid	3
2MASS J02055138−0759253	L2	85	mid	42
2MASSW J0944027+313132	L2	86	mid	3
2MASS J20414283−3506442	L2	88	mid	3
2MASSI J0241536−124106	L2	88	mid	16
SDSS J12061049+6242572	L2	88	mid	3
2MASS J00332386−1521309	L2	90	mid	2
2MASS J13204427+0409045	L2	92	mid	3
2MASSW J0030438+313932	L2	99	mid	3
2MASS J01311838+3801554	L2	99	mid	19
2MASS J16231308+3950419	L2	99	mid	39
2MASSI J0847287−153237	L2	101	high	57
EROS−MP J0032−4405	L2	104	high	2
SDSS J11594072+5409386	L2	110	high	3
2MASSW J0928397−160312	L2	112	high	3
2MASSW J0135358+120522	L2	113	high	3
2MASSI J0125369−343505	L2	114	high	3
2MASSI J0006205−172051	L2	116	high	3
2MASS J2325560−025950	L2	116	high	19
2MASSI J0316451−284852	L2	120	high	3
2MASSI J0453264−175154	L2	120	high	3
2MASSW J0829066+145622	L2	127	high	3
SDSS J15124067+3403501	L2	130	high	3
2MASS J12312141+4959234	L2	132	high	3

Table 9 *continued on next page*

Table 9 (*continued*)

SIMBAD Name	SpT	S/N	S/N Class	Ref
2MASS J16452207+3004071	L2	136	high	19
2MASS J17111353+2326333	L2	137	high	21
2MASS J02192196+0506306	L2	144	high	3
2MASS J06022216+6336391	L2	144	high	3
G 73–26B	L2	149	high	30
2MASS J11544223–3400390	L2	152	high	3
2MASS J08230838+6125208	L2	159	high	3
2MASSW J1411175+393636	L2	165	high	3
2MASS J12565688+0146163	L2	169	high	3
2MASSW J0208183+254253	L2	171	high	16
SDSS J15512086+4329303	L2	184	high	3
DENIS–P J1058.7–1548	L2	185	high	19
2MASS J07231462+5727081	L2	189	high	3
2MASSW J0141032+180450	L2	193	high	3
2MASSI J1017075+130839	L2	195	high	3
2MASS J02271036–1624479	L2	198	high	16
2MASSW J1552591+294849	L2	198	high	3
SDSS J13271521+0759375	L2	199	high	3
DENIS–P J0812316–244442	L2	203	high	3
GJ 1048B	L2	228	high	16
2MASSW J0015447+351603	L2	231	high	3
2MASS J20360316+1051295	L2	242	high	19
2MASS J23004411+0200105	L3	26	low	40
2MASS J10293958+5715445	L3	29	low	45
2MASS J13571237+1428398	L3	32	low	19
2MASS J00521232+0012172	L3	36	low	58
2MASS J17164260+2945536	L3	37	low	34
2MASS J16231308+3950419	L3	41	low	39
BRLT 105	L3	45	low	40
2MASS J15422494+5522451	L3	49	low	34
2MASS J00150673+3006004	L3	50	mid	40
SDSS J161459.98+400435.1	L3	52	mid	70
WISE J01581203+3231579	L3	53	mid	45
2MASS J07575274+0914103	L3	67	mid	3
2MASS J01414428+2227409	L3	68	mid	40
2MASS J10461875+4441149	L3	68	mid	42
2MASS J07244848+2506143	L3	73	mid	40
GD 165B	L3	76	mid	3
2MASSW J1122362–391605	L3	78	mid	3
WISE J223552.24+041854.7	L3	79	mid	40
2MASS J21203387–0747208	L3	80	mid	39
2MASSW J1438549–130910	L3	80	mid	3
2MASS J23271573+1517310	L3	83	mid	62
SDSS J143832.63+572216.9	L3	92	mid	3
2MASS J23313131+2041273	L3	106	high	40
SDSS J125128.43+624310.7	L3	107	high	3
2MASSI J0409095+210439	L3	119	high	3

Table 9 *continued on next page*

Table 9 (*continued*)

SIMBAD Name	SpT	S/N	S/N Class	Ref
2MASSI J0218291-313322	L3	129	high	3
2MASSW J1506544+132106	L3	131	high	13
2MASS J18000116-1559235	L3	153	high	3
2MASS J14283132+5923354	L3	166	high	19
2MASS J00531899-3631102	L3	169	high	19
SDSSp J053951.99-005902	L3	170	high	23
2MASSW J1615441+355900	L3	184	high	3
2MASS J03250136+2253039	L3	188	high	3
SDSSp J120358.19+001550.3	L3	194	high	3
WISE J040137.21+284951.7	L3	266	high	20
WISE J05500794+1610519	L3	297	high	44
2MASSW J1507476-162738	L4	41	low	13
2MASS J16370238+2520386	L4	43	low	39
2MASS J17392515+2454421	L4	46	low	42
2MASSW J1515008+484742	L4	50	mid	19
SDSSp J033035.13-002534.5	L4	51	mid	3
SDSS J163359.23-064056.5	L4	55	mid	21
2MASS J17461199+5034036	L4	57	mid	19
PSO J023.8557+02.0884	L4	65	mid	40
2MASS J14140586+0107102	L4	69	mid	34
2MASSI J0908380+503208	L4	72	mid	69
2MASS J03001631+2130205	L4	79	mid	42
2MASS J18131803+5101246	L4	81	mid	42
SDSSp J125737.26-011336.1	L4	89	mid	3
2MASSI J1213033-043243	L4	102	high	3
2MASS J21580457-1550098	L4	102	high	3
2MASSI J1104012+195921	L4	102	high	8
WISE J165842.56+510335	L4	109	high	3
SDSS J16260303+2113130	L4	124	high	3
2MASSI J0443058-320209	L4	138	high	3
2MASS J23440624-0733282	L4	148	high	3
2MASS J17502484-0016151	L4	153	high	19
LHS 5166B	L4	167	high	3
2MASSI J0439010-235308	L5	0	low	13
2MASS J09054654+5623117	L5	14	low	19
WISE J04364275+1901348	L5	25	low	67
WISEA J205202.06-204313	L5	35	low	66
WISE J03244023-1919056	L5	40	low	67
2MASS J221912830+11134060	L5	43	low	40
PSO J334.8034+11.2278	L5	49	low	5
2MASS J14261286+3130394	L5	50	mid	3
2MASS J13331605+3744214	L5	52	mid	45
SDSS J074838.61+174332.9	L5	54	mid	3
2MASS J01550354+0950003	L5	57	mid	19
SDSS J012743.51+135420.9	L5	62	mid	3
2MASS J12172372-0237369	L5	63	mid	34
2MASSW J0801405+462850	L5	64	mid	19

Table 9 *continued on next page*

Table 9 (*continued*)

SIMBAD Name	SpT	S/N	S/N Class	Ref
SDSSp J144600.60+002452	L5	65	mid	3
2MASSI J0013578-223520	L5	69	mid	3
2MASS J11191046+0552484	L5	73	mid	34
2MASS J01183399+1810542	L5	77	mid	40
SDSS J104409.43+042937.6	L5	90	mid	19
SDSS J104922.45+012559.2	L5	92	mid	3
2MASSI J1526140+204341	L5	95	mid	8
SDSS J115553.86+055957.5	L5	95	mid	19
2MASSW J0208549+250048	L5	102	high	3
2MASSW J0326137+295015	L5	115	high	3
2MASSW J1246467+402715	L5	115	high	3
SDSS J153453.33+121949.2	L5	124	high	21
GJ 499C	L5	135	high	3
2MASS J18212815+1414010	L5	167	high	48
2MASS J05002100+0330501	L5	331	high	3
WISE J060738.65+242953.5	L5	405	high	70
2MASS J13042886-0032410	L6	24	low	40
WISE J07053400-1839256	L6	24	low	67
2MASS J11000965+4957470	L6	26	low	69
2MASS J13451417+4757231	L6	27	low	40
2MASS J05161597-3332046	L6	28	low	19
2MASS J23254530+4251488	L6	28	low	19
2MASS J15565004+1449081	L6	30	low	40
WISE J23333346+0251284	L6	33	low	67
2MASS J11260310+4819256	L6	33	low	39
BRLT 171	L6	33	low	40
SDSS J102552.43+321234	L6	33	low	21
PSO J127.4696+10.5777	L6	34	low	5
2MASS J09325053+1836485	L6	34	low	40
2MASS J11220855+0343193	L6	35	low	40
WISE J12222195-2139486	L6	37	low	66
2MASS J00150206+2959323	L6	37	low	42
2MASS J0028208+224905	L6	38	low	19
2MASS J15500191+4500451	L6	40	low	40
2MASS J23392527+3507165	L6	41	low	19
PSO J344.8146+20.1917	L6	43	low	5
SDSS J134203.11+134022.2	L6	43	low	21
2MASSW J0129122+351758	L6	44	low	3
WISEA J130729.56-055815.4	L6	45	low	66
WISE J19072256+4727453	L6	48	low	67
2MASSW J0708213+295035	L6	48	low	3
2MASS J01392388-1845029	L6	49	low	40
2MASS J15111091+4340363	L6	50	mid	3
2MASS J17120142+3108217	L6	51	mid	40
2MASS J21513979+3402444	L6	52	mid	42
2MASS J13184794+1736117	L6	54	mid	42
2MASS J15543602+2724487	L6	55	mid	40

Table 9 *continued on next page*

Table 9 (*continued*)

SIMBAD Name	SpT	S/N	S/N Class	Ref
2MASS J02572581-3105523	L6	55	mid	69
2MASS J01165802+4333081	L6	57	mid	40
2MASS J03101401-2756452	L6	60	mid	3
2MASS J16005759+3021571	L6	62	mid	39
2MASS J12070374-3151298	L6	73	mid	69
2MASSW J1743415+212707	L6	74	mid	3
2MASS J19285196-4356256	L6	75	mid	19
2MASSI J1010148-040649	L6	81	mid	61
SDSS J001608.44-004302.3	L6	83	mid	3
2MASSI J0302012+135814	L6	86	mid	3
2MASSW J0208236+273740	L6	87	mid	19
2MASS J14402290+1339230	L6	92	mid	62
2MASS J00165953-4056541	L6	99	mid	19
GJ 618.1B	L6	105	high	3
WISE J173332.50+314458.3	L6	105	high	70
2MASSW J0918382+213406	L6	106	high	3
2MASSI J0034568-070601	L6	112	high	3
2MASSW J0355419+225702	L6	112	high	3
2MASS J08234818+2428577	L6	113	high	19
SDSSp J032817.38+003257.2	L6	113	high	3
2MASSW J0740096+321203	L6	113	high	3
WISE J080700.23+413026.8	L6	115	high	70
2MASS J04070752+1546457	L6	119	high	16
2MASSW J0309088-194938	L6	122	high	3
2MASS J14075361+1241099	L6	125	high	19
2MASSW J0051107-154417	L6	137	high	19
2MASSW J1448256+103159	L6	141	high	19
WISE J040418.01+412735.6	L6	147	high	20
2MASS J22425317+2542573	L6	164	high	19
2MASSI J1029216+162652	L6	174	high	3
2MASS J11472421-2040204	L7	18	low	65
WISE J00440339+0228106	L7	23	low	67
2MASSI J0103320+193536	L7	24	low	22
WISE J14321117+3244338	L7	25	low	67
WISE J173859.27+614242.1	L7	25	low	56
WISE J00062785+1857288	L7	26	low	66
WISE J151314.61+401935.6	L7	26	low	70
WISE J02022929+2305139	L7	28	low	67
PSO J004.7148+51.8918	L7	29	low	5
2MASS J01262109+1428057	L7	29	low	58
2MASS J15382417-1953116	L7	30	low	31
WISE J13184558+3626140	L7	35	low	67
WISE J14564268+6450097	L7	36	low	67
2MASS J00440332+0228112	L7	37	low	40
2MASS J03530419+0418193	L7	38	low	40
2MASS J0447430-193604	L7	38	low	19
2MASS J00550564+0134365	L7	38	low	31

Table 9 *continued on next page*

Table 9 (*continued*)

SIMBAD Name	SpT	S/N	S/N Class	Ref
2MASS J16135698+4019158	L7	39	low	39
2MASS J23352734+4511442	L7	40	low	5
2MASSW J0820299+450031	L7	41	low	19
2MASSW J0306268+154514	L7	41	low	3
LP 261-75B	L7	41	low	7
2MASSW J1553214+210907	L7	41	low	3
2MASSW J0929336+342952	L7	41	low	19
2MASS J20025073-0521524	L7	42	low	16
2MASS J03185403-3421292	L7	42	low	19
2MASSW J0829570+265510	L7	43	low	3
WISE J164715.57+563208.3	L7	45	low	43
2MASS J21163374-0729200	L7	46	low	34
SDSSp J132629.82-003831.5	L7	46	low	19
WISE J032301.86+562558	L7	48	low	53
2MASSW J1343167+394508	L7	51	mid	3
SDSS J151506.11+443648.3	L7	53	mid	19
2MASS J04354290+1323449	L7	55	mid	5
2MASS J03264225-2102057	L7	56	mid	33
WISE J07235262-3309435	L7	59	mid	67
WISE J020625.27+264023.6	L7	59	mid	43
WISE J095729.41+462413.5	L7	63	mid	53
WISE J09025899+6708331	L7	63	mid	67
2MASSI J0028394+150141	L7	64	mid	3
2MASSW J0337036-175807	L7	64	mid	3
2MASS J05120636-2949540	L7	64	mid	3
2MASS J09593276+4523309	L7	66	mid	31
SDSS J080959.01+443422.2	L7	66	mid	3
WISEP J004701.06+680352.1	L7	68	mid	38
2MASSW J1326201-272937	L7	69	mid	3
WISE J174102.78-464225.5	L7	71	mid	64
2MASSW J2244316+204343	L7	74	mid	48
2MASSI J0835425-081923	L7	77	mid	19
2MASS J17081563+2557474	L7	79	mid	39
2MASS J21512543-2441000	L7	84	mid	16
2MASSW J1328550+211449	L7	88	mid	3
2MASS J23512200+3010540	L7	92	mid	42
2MASS J23174712-4838501	L7	97	mid	42
2MASS J03582213-4116144	L7	107	high	33
2MASS J05012406-0010452	L7	108	high	31
SDSSp J010752.33+004156.1	L7	110	high	3
2MASSI J0825196+211552	L7	117	high	19
2MASSW J0717163+570543	L7	128	high	19
2MASSW J0205034+125142	L7	130	high	60
SDSSp J085758.45+570851.4	L7	142	high	19
SDSS J171714.10+652622.2	L7	147	high	3
2MASS J21481628+4003593	L7	156	high	48
2MASSW J2224438-015852	L7	157	high	19

Table 9 *continued on next page*

Table 9 (*continued*)

SIMBAD Name	SpT	S/N	S/N Class	Ref
2MASS J01443536-0716142	L7	188	high	16
DENIS-P J142527.97-365023.4	L7	275	high	3
2MASS J10430758+2225236	L8	37	low	69
Gliese 584C	L8	46	low	19
2MASSW J1632291+190441	L8	49	low	8
2MASS J06420559+4101599	L8	50	mid	5
SDSS J163030.53+434404	L8	57	mid	19
SDSS J140023.12+433822.3	L8	67	mid	19
SDSS J121951.45+312849.4	L8	80	mid	19
2MASSI J0859254-194926	L8	125	high	69
WISEP J180026.60+013453.1	L8	211	high	36
WISE J12010457+5730042	L9	25	low	67
SDSS J154009.36+374230.3	L9	28	low	21
WISE J183058.56+454257.4	L9	39	low	43
SDSS J151643.01+305344.4	L9	39	low	19
SDSSp J003259.36+141036.6	L9	41	low	19
SDSS J103026.78+021306.4	L9	41	low	19
SDSS J204749.61-071818.3	L9	48	low	19
2MASS J01453520-0314117	L9	48	low	40
2MASS J21243864+1849263	L9	53	mid	39
WISE J232728.74-273056.6	L9	53	mid	43
WISE J222219.93+302601.4	L9	54	mid	3
SIMP J09560810-1447065	L9	55	mid	62
SDSS J085234.90+472035	L9	56	mid	19
2MASSI J0328426+230205	L9	58	mid	16
SDSSp J083008.12+482847.4	L9	59	mid	16
WISE J003110.04+574936.3	L9	72	mid	4
2MASSW J1036530-344138	L9	81	mid	19
WISE J004928.48+044059.9	L9	81	mid	43
SDSS J104335.08+121314.1	L9	101	high	42
WISE J185101.83+593508.6	L9	110	high	4
SDSS J152039.82+354619.8	L9	119	high	19
DENIS-P J0255-4700	L9	140	high	10
SDSS J024749.90-163112.6	T0	27	low	21
WISE J120035.40-283657.5	T0	30	low	66
PSO J319.3102-29.6682	T0	34	low	5
SDSS J204317.69-155103.4	T0	38	low	21
WISE J00164397+2304265	T0	40	low	66
2MASS J15423630-0045452	T0	41	low	34
SDSS J133148.92-011651.4	T0	43	low	19
WISE J005757.63+201304.2	T0	48	low	44
PSO J004.1834+23.0741	T0	49	low	5
SDSS J020608.97+223559.2	T0	51	mid	21
2MASS J13043568+1542521	T0	61	mid	39
WISE J044633.45-242956.9	T0	66	mid	70
PSO J342.3797-16.4665	T0	72	mid	5
SDSS J09002368+2539343	T0	73	mid	3

Table 9 continued on next page

Table 9 (*continued*)

SIMBAD Name	SpT	S/N	S/N Class	Ref
2MASS J14025564+0800553	T0	86	mid	39
WISE J015010.89+382724.1	T0	97	mid	43
SDSSp J023617.93+004855	T0	102	high	3
2MASS J11263991-5003550	T0	108	high	17
WISE J092055.40+453856.3	T0	143	high	4
PSO J331.6058+33.0207	T1	31	low	5
SDSSp J083717.22-000018.3	T1	54	mid	10
2MASS J23322678+1234530	T1	57	mid	39
WISE J173035.99+420742.1	T1	59	mid	56
SDSS J015141.69+124429.6	T1	73	mid	8
PSO J226.2599-28.8959	T1	85	mid	25
2MASS J11582077+0435014	T1	103	high	42
2MASS J22153705+2110554	T1	164	high	62
2MASS J21392676+0220226	T1	218	high	10
2MASS J14162409+1348267	T1	423	high	63
SDSS J090900.73+652527.2	T2	39	low	21
SDSS J163239.34+415004.3	T2	42	low	19
SDSS J175024.01+422237.8	T2	47	low	10
WISE J204356.42+622049	T2	52	mid	56
WISE J013836.58-032221.2	T2	81	mid	43
SDSSp J125453.90-012247.4	T2	82	mid	8
HN Peg B	T2	114	high	50
PSO J247.3273+03.5932	T2	141	high	27
SDSS J075840.33+324723.4	T2	208	high	16
WISE J203042.79+074934.7	T2	357	high	56
IPMS J013656.57+093347.3	T2	388	high	16
2MASS J15461461+4932114	T3	32	low	58
WISEA J223343.53-133140.9	T3	42	low	66
PSO J334.1193+19.8800	T3	42	low	5
WISE J065609.59+420531.9	T3	46	low	43
WISEA J230329.45+315022.7	T3	53	mid	66
SDSS J152103.24+013142.7	T3	57	mid	19
SDSS J104829.21+091937.8	T3	62	mid	19
SIMP J03162759+2650277	T3	68	mid	62
WISE J175510.28+180320.2	T3	77	mid	53
2MASS J11220826-3512363	T3	95	mid	10
WISE J223937.55+161716.1	T3	105	high	43
2MASS J00132229-1143006	T4	45	low	40
2MASS J10595185+3042059	T4	57	mid	68
2MASS J21513839-4853542	T4	77	mid	10
SDSSp J175032.96+175903.9	T4	88	mid	8
2MASS J21542494-1023022	T4	89	mid	47
WISE J081958.05-033528.5	T4	101	high	43
WISE J173421.04+502350.8	T4	102	high	56
PSO J201.0320+19.1072	T4	124	high	25
2MASSI J2254188+312349	T4	179	high	8
WISE J163236.47+032927.3	T5	26	low	56

Table 9 *continued on next page*

Table 9 (*continued*)

SIMBAD Name	SpT	S/N	S/N Class	Ref
WISE J174113.12+132711.9	T5	27	low	56
WISE J082131.64+144319.2	T5	32	low	43
WISE J223729.52−061434.4	T5	34	low	43
2MASS J23312378−4718274	T5	39	low	8
PSO J246.4222+15.4698	T5	40	low	25
WISE J033651.90+282628.8	T5	41	low	56
LP 738−14B	T5	45	low	25
WISE J023318.05+303030.5	T5	45	low	56
SDSS J135852.68+374711.9	T5	49	low	21
2MASS J0755480+221218	T5	56	mid	10
WISE J054601.19−095947.5	T5	57	mid	56
2MASS J04070885+1514565	T5	64	mid	8
2MASS J2339101+135230	T5	69	mid	10
2MASS J2356547−155310	T5	71	mid	10
WISE J021010.25+400829.6	T5	72	mid	56
WISE J200804.71−083428.5	T5	75	mid	56
HIP 38939B	T5	77	mid	26
PSO J076.7092+52.6087	T5	78	mid	5
2MASS J06020638+4043588	T5	89	mid	47
SDSS J074149.15+235127.5	T5	92	mid	19
2MASS J15462718−3325111	T5	95	mid	16
2MASS J19010601+4718136	T5	95	mid	8
2MASS J05591914−1404488	T5	98	mid	10
WISE J004542.56+361139.1	T5	99	mid	56
SDSS J083048.80+012831.1	T5	107	high	19
SDSS J074201.41+205520.5	T5	124	high	19
2MASS J1754544+164920	T5	130	high	16
2MASS J05160945−0445499	T5	147	high	16
2MASS J15031961+2525196	T5	151	high	8
WISE J223617.59+510551.9	T5	241	high	4
WISE J172134.46+111739.4	T6	21	low	56
WISE J101905.62+652954.2	T6	25	low	43
WISE J172844.93+571642.7	T6	28	low	43
WISE J112254.72+255022.2	T6	29	low	43
WISE J013525.64+171503.4	T6	30	low	56
WISE J125715.90+400854.2	T6	31	low	56
2MASS J10073369−4555147	T6	35	low	47
WISE J052536.35+673952.6	T6	39	low	43
WISE J095259.29+195508.1	T6	41	low	43
2MASS J22282889−4310262	T6	46	low	8
2MASS J18283572−4849046	T6	47	low	8
2MASS J16150413+1340079	T6	48	low	47
WISE J230133.32+021635	T6	48	low	56
WISE J235716.49+122741.8	T6	63	mid	56
WISE J234228.98+085620.2	T6	65	mid	56
WISE J162208.93−095934.4	T6	67	mid	43
WISE J122558.86−101345	T6	74	mid	56

Table 9 *continued on next page*

Table 9 (*continued*)

SIMBAD Name	SpT	S/N	S/N Class	Ref
2MASS J21543318+5942187	T6	77	mid	9
WISE J234026.61-074508.1	T6	85	mid	43
WISE J190624.74+450807.1	T6	90	mid	43
WISE J062720.07-111428	T6	97	mid	43
2MASS J12373919+6526148	T6	106	high	46
2MASSI J0937347+293142	T6	114	high	12
2MASS J12314753+0847331	T6	129	high	8
WISE J162725.65+325524.6	T6	135	high	43
2MASSI J1047538+212423	T6	150	high	16
2MASSI J0243137-245329	T6	169	high	8
WISE J192841.35+235604.9	T6	429	high	56
WISE J024512.62-345047.8	T7	21	low	56
WISE J231939.14-184404.4	T7	22	low	43
WISE J103907.73-160002.9	T7	22	low	56
2MASSI J1217110-031113	T7	26	low	12
WISE J145715.03+581510.2	T7	34	low	43
ULAS J141623.94+134836.3	T7	38	low	18
WISE J132004.16+603426.3	T7	41	low	43
WISE J185215.76+353716.7	T7	43	low	43
WISE J122152.28-313600.8	T7	45	low	56
SDSS J162838.77+230821.1	T7	49	low	28
2MASS J00501994-3322402	T7	54	mid	12
WISE J032547.72+083118.2	T7	55	mid	56
WISE J234841.10-102844.1	T7	57	mid	43
WISE J105257.95-194250.2	T7	61	mid	70
WISE J112438.12-042149.7	T7	64	mid	56
WISE J221354.68+091139.4	T7	67	mid	43
WISE J004024.88+090054.8	T7	72	mid	56
2MASSI J0727182+171001	T7	96	mid	12
WISE J050003.04-122343.2	T8	10	low	43
WISE J180901.07+383805.4	T8	20	low	52
2MASS J11145133-2618235	T8	24	low	12
WISE J165311.05+444422.8	T8	28	low	43
WISE J225540.75-311842	T8	33	low	43
ULAS J102940.52+093514.6	T8	33	low	70
WISE J022322.36-293257.2	T8	41	low	43
HD 3651B	T8	55	mid	15
WISE J222623.05+044004	T8	55	mid	43
WISE J025409.51+022358.6	T8	81	mid	43
2MASSI J0415195-093506	T8	138	high	8
UGPS J072227.51-054031.2	T9	63	mid	71
WISE J004945.61+215120	T9	65	mid	56

Table 9 *continued on next page*

Table 9 (*continued*)

SIMBAD Name	SpT	S/N	S/N Class	Ref
-------------	-----	-----	-----------	-----

References— (1) Aganze et al. (2016); (2) Allers & Liu (2013); (3) Bardalez Gagliuffi et al. (2014); (4) Best et al. (2013); (5) Best et al. (2015); (6) Bowler et al. (2009); (7) Bowler et al. (2013); (8) Burgasser et al. (2004); (9) Burgasser (2004b); (10) Burgasser et al. (2006b); (11) Burgasser & McElwain (2006); (12) Burgasser et al. (2006a); (13) Burgasser (2007a); (14) Burgasser et al. (2007a); (15) Burgasser (2007b); (16) Burgasser et al. (2008a); (17) Burgasser et al. (2008b); (18) Burgasser et al. (2010b); (19) Burgasser et al. (2010a); (20) Castro et al. (2013); (21) Chiu et al. (2006); (22) Cruz et al. (2003); (23) Cushing et al. (2004); (24) Dawson et al. (2014); (25) Deacon et al. (2011); (26) Deacon et al. (2012a); (27) Deacon et al. (2012b); (28) Dupuy & Liu (2012); (29) Esplin et al. (2014); (30) Faherty et al. (2010); (31) Faherty et al. (2016); (32) Gagné et al. (2014); (33) Gagné et al. (2015); (34) Geiffler et al. (2011); (35) Gillon et al. (2016); (36) Gizis et al. (2011a); (37) Gizis et al. (2011b); (38) Gizis et al. (2012); (39) Kellogg et al. (2015); (40) Kellogg et al. (2017); (41) Kirkpatrick et al. (2008); (42) Kirkpatrick et al. (2010); (43) Kirkpatrick et al. (2011); (44) Kirkpatrick et al. (2014); (45) Kirkpatrick et al. (2016); (46) Liebert & Burgasser (2007); (47) Looper et al. (2007b); (48) Looper et al. (2008); (49) Luhman et al. (2006); (50) Luhman et al. (2007); (51) Luhman et al. (2009); (52) Luhman et al. (2012); (53) Luhman & Sheppard (2014); (54) Luhman et al. (2016); (55) Luhman et al. (2017); (56) Mace et al. (2013); (57) McElwain & Burgasser (2006); (58) Metchev et al. (2008); (59) Muench et al. (2007); (60) Reid et al. (2006b); (61) Reid et al. (2006a); (62) Robert et al. (2016); (63) Schmidt et al. (2010); (64) Schneider et al. (2014); (65) Schneider et al. (2016b); (66) Schneider et al. (2016a); (67) Schneider et al. (2017); (68) Sheppard & Cushing (2009); (69) Siegler et al. (2007); (70) Thompson et al. (2013); (71) Burgasser & Splat Development Team (2017).

REFERENCES

- Aganze, C., Burgasser, A. J., Faherty, J. K., et al. 2016, *AJ*, 151, 46, doi: [10.3847/0004-6256/151/2/46](https://doi.org/10.3847/0004-6256/151/2/46)
- Aganze, C., Burgasser, A. J., Malkan, M., et al. 2022, *ApJ*, 924, 114, doi: [10.3847/1538-4357/ac35ea](https://doi.org/10.3847/1538-4357/ac35ea)
- Allers, K. N., & Liu, M. C. 2013, *ApJ*, 772, 79, doi: [10.1088/0004-637X/772/2/79](https://doi.org/10.1088/0004-637X/772/2/79)
- Allers, K. N., Liu, M. C., Dupuy, T. J., & Cushing, M. C. 2010, *ApJ*, 715, 561, doi: [10.1088/0004-637X/715/1/561](https://doi.org/10.1088/0004-637X/715/1/561)
- Angthopo, J., Granett, B. R., La Barbera, F., et al. 2024, *A&A*, 690, A198, doi: [10.1051/0004-6361/202449979](https://doi.org/10.1051/0004-6361/202449979)
- Ashraf, A., Bardalez Gagliuffi, D. C., Manjavacas, E., et al. 2022, *ApJ*, 934, 178, doi: [10.3847/1538-4357/ac7aab](https://doi.org/10.3847/1538-4357/ac7aab)
- Astropy Collaboration, Robitaille, T. P., Tollerud, E. J., et al. 2013, *A&A*, 558, A33, doi: [10.1051/0004-6361/201322068](https://doi.org/10.1051/0004-6361/201322068)
- Astropy Collaboration, Price-Whelan, A. M., Sipőcz, B. M., et al. 2018, *AJ*, 156, 123, doi: [10.3847/1538-3881/aabc4f](https://doi.org/10.3847/1538-3881/aabc4f)
- Astropy Collaboration, Price-Whelan, A. M., Lim, P. L., et al. 2022, *ApJ*, 935, 167, doi: [10.3847/1538-4357/ac7c74](https://doi.org/10.3847/1538-4357/ac7c74)
- Baraffe, I., Chabrier, G., Barman, T. S., Allard, F., & Hauschildt, P. H. 2003, *A&A*, 402, 701, doi: [10.1051/0004-6361:20030252](https://doi.org/10.1051/0004-6361:20030252)
- Bardalez Gagliuffi, D. C. 2017, PhD thesis, University of California, San Diego
- Bardalez Gagliuffi, D. C., Gelino, C. R., & Burgasser, A. J. 2015, *AJ*, 150, 163, doi: [10.1088/0004-6256/150/5/163](https://doi.org/10.1088/0004-6256/150/5/163)

- Bardalez Gagliuffi, D. C., Burgasser, A. J., Gelino, C. R., et al. 2014, *ApJ*, 794, 143, doi: [10.1088/0004-637X/794/2/143](https://doi.org/10.1088/0004-637X/794/2/143)
- Bardalez Gagliuffi, D. C., Burgasser, A. J., Schmidt, S. J., et al. 2019a, *ApJ*, 883, 205, doi: [10.3847/1538-4357/ab253d](https://doi.org/10.3847/1538-4357/ab253d)
- . 2019b, *ApJ*, 883, 205, doi: [10.3847/1538-4357/ab253d](https://doi.org/10.3847/1538-4357/ab253d)
- Baron, D. 2019, arXiv e-prints, arXiv:1904.07248, doi: [10.48550/arXiv.1904.07248](https://doi.org/10.48550/arXiv.1904.07248)
- Basri, G., & Martín, E. L. 1999, *AJ*, 118, 2460, doi: [10.1086/301079](https://doi.org/10.1086/301079)
- Beiler, S. A., Cushing, M. C., Kirkpatrick, J. D., et al. 2024, *ApJ*, 973, 107, doi: [10.3847/1538-4357/ad6301](https://doi.org/10.3847/1538-4357/ad6301)
- Best, W. M. J., Dupuy, T. J., Liu, M. C., et al. 2024, The UltracoolSheet: Photometry, Astrometry, Spectroscopy, and Multiplicity for 4000+ Ultracool Dwarfs and Imaged Exoplanets, 2.0.0, Zenodo, doi: [10.5281/zenodo.10573247](https://doi.org/10.5281/zenodo.10573247)
- Best, W. M. J., Liu, M. C., Dupuy, T. J., & Magnier, E. A. 2017, *ApJL*, 843, L4, doi: [10.3847/2041-8213/aa76df](https://doi.org/10.3847/2041-8213/aa76df)
- Best, W. M. J., Sanghi, A., Liu, M. C., Magnier, E. A., & Dupuy, T. J. 2024, *ApJ*, 967, 115, doi: [10.3847/1538-4357/ad39ef](https://doi.org/10.3847/1538-4357/ad39ef)
- Best, W. M. J., Liu, M. C., Magnier, E. A., et al. 2013, *ApJ*, 777, 84, doi: [10.1088/0004-637X/777/2/84](https://doi.org/10.1088/0004-637X/777/2/84)
- . 2015, *ApJ*, 814, 118, doi: [10.1088/0004-637X/814/2/118](https://doi.org/10.1088/0004-637X/814/2/118)
- Blake, C. H., Charbonneau, D., White, R. J., Marley, M. S., & Saumon, D. 2007, *ApJ*, 666, 1198, doi: [10.1086/520124](https://doi.org/10.1086/520124)
- Blake, C. H., Charbonneau, D., White, R. J., et al. 2008, *ApJL*, 678, L125, doi: [10.1086/588754](https://doi.org/10.1086/588754)
- Bowler, B. P., Liu, M. C., & Cushing, M. C. 2009, *ApJ*, 706, 1114, doi: [10.1088/0004-637X/706/2/1114](https://doi.org/10.1088/0004-637X/706/2/1114)
- Bowler, B. P., Liu, M. C., Shkolnik, E. L., & Dupuy, T. J. 2013, *ApJ*, 774, 55, doi: [10.1088/0004-637X/774/1/55](https://doi.org/10.1088/0004-637X/774/1/55)
- Bravo, A., Schneider, A. C., Bardalez Gagliuffi, D., et al. 2023, *AJ*, 166, 226, doi: [10.3847/1538-3881/acffc1](https://doi.org/10.3847/1538-3881/acffc1)
- Breiman, L. 2001, *Machine Learning*, 45, 5, doi: [10.1023/A:1010933404324](https://doi.org/10.1023/A:1010933404324)
- Burgasser, A., Theissen, C., ttamiya, et al. 2025, aburgasser/splat: v1.11, v1.11, Zenodo, doi: [10.5281/zenodo.17107529](https://doi.org/10.5281/zenodo.17107529)
- Burgasser, A. J. 2004a, *ApJS*, 155, 191, doi: [10.1086/424386](https://doi.org/10.1086/424386)
- . 2004b, *ApJL*, 614, L73, doi: [10.1086/425418](https://doi.org/10.1086/425418)
- . 2007a, *ApJ*, 659, 655, doi: [10.1086/511027](https://doi.org/10.1086/511027)
- . 2007b, *ApJ*, 658, 617, doi: [10.1086/511176](https://doi.org/10.1086/511176)
- Burgasser, A. J., Bardalez-Gagliuffi, D. C., & Gizis, J. E. 2011a, *AJ*, 141, 70, doi: [10.1088/0004-6256/141/3/70](https://doi.org/10.1088/0004-6256/141/3/70)
- Burgasser, A. J., Burrows, A., & Kirkpatrick, J. D. 2006a, *ApJ*, 639, 1095, doi: [10.1086/499344](https://doi.org/10.1086/499344)
- Burgasser, A. J., Cruz, K. L., Cushing, M., et al. 2010a, *ApJ*, 710, 1142, doi: [10.1088/0004-637X/710/2/1142](https://doi.org/10.1088/0004-637X/710/2/1142)
- Burgasser, A. J., Dhital, S., & West, A. A. 2009, *AJ*, 138, 1563, doi: [10.1088/0004-6256/138/6/1563](https://doi.org/10.1088/0004-6256/138/6/1563)
- Burgasser, A. J., Geballe, T. R., Leggett, S. K., Kirkpatrick, J. D., & Golimowski, D. A. 2006b, *ApJ*, 637, 1067, doi: [10.1086/498563](https://doi.org/10.1086/498563)
- Burgasser, A. J., Gelino, C. R., Cushing, M. C., & Kirkpatrick, J. D. 2012a, *ApJ*, 745, 26, doi: [10.1088/0004-637X/745/1/26](https://doi.org/10.1088/0004-637X/745/1/26)
- Burgasser, A. J., Kirkpatrick, J. D., Cruz, K. L., et al. 2006c, *ApJS*, 166, 585, doi: [10.1086/506327](https://doi.org/10.1086/506327)
- Burgasser, A. J., Kirkpatrick, J. D., Reid, I. N., et al. 2003, *ApJ*, 586, 512, doi: [10.1086/346263](https://doi.org/10.1086/346263)
- Burgasser, A. J., Liu, M. C., Ireland, M. J., Cruz, K. L., & Dupuy, T. J. 2008a, *ApJ*, 681, 579, doi: [10.1086/588379](https://doi.org/10.1086/588379)
- Burgasser, A. J.,Looper, D., & Rayner, J. T. 2010b, *AJ*, 139, 2448, doi: [10.1088/0004-6256/139/6/2448](https://doi.org/10.1088/0004-6256/139/6/2448)

- Burgasser, A. J., Looper, D. L., Kirkpatrick, J. D., Cruz, K. L., & Swift, B. J. 2008b, *ApJ*, 674, 451, doi: [10.1086/524726](https://doi.org/10.1086/524726)
- Burgasser, A. J., Looper, D. L., Kirkpatrick, J. D., & Liu, M. C. 2007a, *ApJ*, 658, 557, doi: [10.1086/511518](https://doi.org/10.1086/511518)
- Burgasser, A. J., Luk, C., Dhital, S., et al. 2012b, *ApJ*, 757, 110, doi: [10.1088/0004-637X/757/2/110](https://doi.org/10.1088/0004-637X/757/2/110)
- Burgasser, A. J., & McElwain, M. W. 2006, *AJ*, 131, 1007, doi: [10.1086/499042](https://doi.org/10.1086/499042)
- Burgasser, A. J., McElwain, M. W., Kirkpatrick, J. D., et al. 2004, *AJ*, 127, 2856, doi: [10.1086/383549](https://doi.org/10.1086/383549)
- Burgasser, A. J., Reid, I. N., Siegler, N., et al. 2007b, in *Protostars and Planets V*, ed. B. Reipurth, D. Jewitt, & K. Keil, 427, doi: [10.48550/arXiv.astro-ph/0602122](https://doi.org/10.48550/arXiv.astro-ph/0602122)
- Burgasser, A. J., Sitarski, B. N., Gelino, C. R., Logsdon, S. E., & Perrin, M. D. 2011b, *ApJ*, 739, 49, doi: [10.1088/0004-637X/739/1/49](https://doi.org/10.1088/0004-637X/739/1/49)
- Burgasser, A. J., & Splat Development Team. 2017, in *Astronomical Society of India Conference Series*, Vol. 14, *Astronomical Society of India Conference Series*, 7–12. <https://arxiv.org/abs/1707.00062>
- Burgasser, A. J., Tinney, C. G., Cushing, M. C., et al. 2008c, *ApJL*, 689, L53, doi: [10.1086/595747](https://doi.org/10.1086/595747)
- Burgasser, A. J., Gillon, M., Melis, C., et al. 2015, *AJ*, 149, 104, doi: [10.1088/0004-6256/149/3/104](https://doi.org/10.1088/0004-6256/149/3/104)
- Castro, P. J., Gizis, J. E., Harris, H. C., et al. 2013, *ApJ*, 776, 126, doi: [10.1088/0004-637X/776/2/126](https://doi.org/10.1088/0004-637X/776/2/126)
- Chen, S.-X., Sun, W.-M., & He, Y. 2022, *Research in Astronomy and Astrophysics*, 22, 025017, doi: [10.1088/1674-4527/ac41c5](https://doi.org/10.1088/1674-4527/ac41c5)
- Chiu, K., Fan, X., Leggett, S. K., et al. 2006, *AJ*, 131, 2722, doi: [10.1086/501431](https://doi.org/10.1086/501431)
- Cruz, K. L., Burgasser, A. J., Reid, I. N., & Liebert, J. 2004a, *ApJL*, 604, L61, doi: [10.1086/383415](https://doi.org/10.1086/383415)
- . 2004b, *ApJL*, 604, L61, doi: [10.1086/383415](https://doi.org/10.1086/383415)
- Cruz, K. L., Reid, I. N., Liebert, J., Kirkpatrick, J. D., & Lowrance, P. J. 2003, *AJ*, 126, 2421, doi: [10.1086/378607](https://doi.org/10.1086/378607)
- Cushing, M. C., Rayner, J. T., & Vacca, W. D. 2005, *ApJ*, 623, 1115, doi: [10.1086/428040](https://doi.org/10.1086/428040)
- Cushing, M. C., Vacca, W. D., & Rayner, J. T. 2004, *PASP*, 116, 362, doi: [10.1086/382907](https://doi.org/10.1086/382907)
- Dawson, P., Scholz, A., Ray, T. P., et al. 2014, *MNRAS*, 442, 1586, doi: [10.1093/mnras/stu973](https://doi.org/10.1093/mnras/stu973)
- Deacon, N. R., Liu, M. C., Magnier, E. A., et al. 2011, *AJ*, 142, 77, doi: [10.1088/0004-6256/142/3/77](https://doi.org/10.1088/0004-6256/142/3/77)
- . 2012a, *ApJ*, 755, 94, doi: [10.1088/0004-637X/755/2/94](https://doi.org/10.1088/0004-637X/755/2/94)
- . 2012b, *ApJ*, 757, 100, doi: [10.1088/0004-637X/757/1/100](https://doi.org/10.1088/0004-637X/757/1/100)
- Deacon, N. R., Magnier, E. A., Best, W. M. J., et al. 2017, *MNRAS*, 468, 3499, doi: [10.1093/mnras/stx440](https://doi.org/10.1093/mnras/stx440)
- Desai, M., Giannoni, J. D. D., Dunning, C., et al. 2023, *Research Notes of the AAS*, 7, 13, doi: [10.3847/2515-5172/acb54a](https://doi.org/10.3847/2515-5172/acb54a)
- Dhital, S., Burgasser, A. J., Looper, D. L., & Stassun, K. G. 2011, *AJ*, 141, 7, doi: [10.1088/0004-6256/141/1/7](https://doi.org/10.1088/0004-6256/141/1/7)
- Dominguez-Tagle, C., Žerjal, M., Sedighi, N., et al. 2025, *ApJ*, 991, 84, doi: [10.3847/1538-4357/adf72d](https://doi.org/10.3847/1538-4357/adf72d)
- Doré, O., Bock, J., Ashby, M., et al. 2014, *arXiv e-prints*, arXiv:1412.4872, doi: [10.48550/arXiv.1412.4872](https://doi.org/10.48550/arXiv.1412.4872)
- Dupuy, T. J., & Liu, M. C. 2012, *ApJS*, 201, 19, doi: [10.1088/0067-0049/201/2/19](https://doi.org/10.1088/0067-0049/201/2/19)
- . 2017, *ApJS*, 231, 15, doi: [10.3847/1538-4365/aa5e4c](https://doi.org/10.3847/1538-4365/aa5e4c)
- Dupuy, T. J., Liu, M. C., Leggett, S. K., et al. 2015, *ApJ*, 805, 56, doi: [10.1088/0004-637X/805/1/56](https://doi.org/10.1088/0004-637X/805/1/56)
- Esplin, T. L., Luhman, K. L., & Mamajek, E. E. 2014, *ApJ*, 784, 126, doi: [10.1088/0004-637X/784/2/126](https://doi.org/10.1088/0004-637X/784/2/126)

- Faherty, J. K., Burgasser, A. J., West, A. A., et al. 2010, *AJ*, 139, 176, doi: [10.1088/0004-6256/139/1/176](https://doi.org/10.1088/0004-6256/139/1/176)
- Faherty, J. K., Riedel, A. R., Cruz, K. L., et al. 2016, *ApJS*, 225, 10, doi: [10.3847/0067-0049/225/1/10](https://doi.org/10.3847/0067-0049/225/1/10)
- Feeser, S. J., & Best, W. M. J. 2022, *MNRAS*, 513, 516, doi: [10.1093/mnras/stac855](https://doi.org/10.1093/mnras/stac855)
- Fontanive, C., Biller, B., Bonavita, M., & Allers, K. 2018, *MNRAS*, 479, 2702, doi: [10.1093/mnras/sty1682](https://doi.org/10.1093/mnras/sty1682)
- Gagné, J., Faherty, J. K., Cruz, K., et al. 2014, *ApJL*, 785, L14, doi: [10.1088/2041-8205/785/1/L14](https://doi.org/10.1088/2041-8205/785/1/L14)
- Gagné, J., Faherty, J. K., Cruz, K. L., et al. 2015, *ApJS*, 219, 33, doi: [10.1088/0067-0049/219/2/33](https://doi.org/10.1088/0067-0049/219/2/33)
- García-Zamora, E. M., Torres, S., & Rebassa-Mansergas, A. 2023, *A&A*, 679, A127, doi: [10.1051/0004-6361/202347601](https://doi.org/10.1051/0004-6361/202347601)
- Geißler, K., Metchev, S., Kirkpatrick, J. D., Berriman, G. B., &Looper, D. 2011, *ApJ*, 732, 56, doi: [10.1088/0004-637X/732/1/56](https://doi.org/10.1088/0004-637X/732/1/56)
- Gelino, C. R., & Burgasser, A. J. 2010, *AJ*, 140, 110, doi: [10.1088/0004-6256/140/1/110](https://doi.org/10.1088/0004-6256/140/1/110)
- Gelino, C. R., Smart, R. L., Marocco, F., et al. 2014, *AJ*, 148, 6, doi: [10.1088/0004-6256/148/1/6](https://doi.org/10.1088/0004-6256/148/1/6)
- Gillon, M., Jehin, E., Lederer, S. M., et al. 2016, *Nature*, 533, 221, doi: [10.1038/nature17448](https://doi.org/10.1038/nature17448)
- Gizis, J. E., Burgasser, A. J., Faherty, J. K., Castro, P. J., & Shara, M. M. 2011a, *AJ*, 142, 171, doi: [10.1088/0004-6256/142/5/171](https://doi.org/10.1088/0004-6256/142/5/171)
- Gizis, J. E., Troup, N. W., & Burgasser, A. J. 2011b, *ApJL*, 736, L34, doi: [10.1088/2041-8205/736/2/L34](https://doi.org/10.1088/2041-8205/736/2/L34)
- Gizis, J. E., Faherty, J. K., Liu, M. C., et al. 2012, *AJ*, 144, 94, doi: [10.1088/0004-6256/144/4/94](https://doi.org/10.1088/0004-6256/144/4/94)
- Harris, C. R., Millman, K. J., van der Walt, S. J., et al. 2020, *Nature*, 585, 357, doi: [10.1038/s41586-020-2649-2](https://doi.org/10.1038/s41586-020-2649-2)
- Hsu, C.-C., Burgasser, A. J., Theissen, C. A., et al. 2021, *ApJS*, 257, 45, doi: [10.3847/1538-4365/ac1c7d](https://doi.org/10.3847/1538-4365/ac1c7d)
- Hunter, J. D. 2007, *Comp. Sci. & Eng.*, 9, 90, doi: [10.1109/MCSE.2007.55](https://doi.org/10.1109/MCSE.2007.55)
- Joergens, V. 2008, *A&A*, 492, 545, doi: [10.1051/0004-6361:200810413](https://doi.org/10.1051/0004-6361:200810413)
- Kellogg, K., Metchev, S., Geißler, K., et al. 2015, *AJ*, 150, 182, doi: [10.1088/0004-6256/150/6/182](https://doi.org/10.1088/0004-6256/150/6/182)
- Kellogg, K., Metchev, S., Miles-Páez, P. A., & Tannock, M. E. 2017, *AJ*, 154, 112, doi: [10.3847/1538-3881/aa83b0](https://doi.org/10.3847/1538-3881/aa83b0)
- Kirkpatrick, J. D., Cruz, K. L., Barman, T. S., et al. 2008, *ApJ*, 689, 1295, doi: [10.1086/592768](https://doi.org/10.1086/592768)
- Kirkpatrick, J. D., Looper, D. L., Burgasser, A. J., et al. 2010, *ApJS*, 190, 100, doi: [10.1088/0067-0049/190/1/100](https://doi.org/10.1088/0067-0049/190/1/100)
- Kirkpatrick, J. D., Cushing, M. C., Gelino, C. R., et al. 2011, *ApJS*, 197, 19, doi: [10.1088/0067-0049/197/2/19](https://doi.org/10.1088/0067-0049/197/2/19)
- Kirkpatrick, J. D., Schneider, A., Fajardo-Acosta, S., et al. 2014, *ApJ*, 783, 122, doi: [10.1088/0004-637X/783/2/122](https://doi.org/10.1088/0004-637X/783/2/122)
- Kirkpatrick, J. D., Kellogg, K., Schneider, A. C., et al. 2016, *ApJS*, 224, 36, doi: [10.3847/0067-0049/224/2/36](https://doi.org/10.3847/0067-0049/224/2/36)
- Kirkpatrick, J. D., Martin, E. C., Smart, R. L., et al. 2019, *ApJS*, 240, 19, doi: [10.3847/1538-4365/aaf6af](https://doi.org/10.3847/1538-4365/aaf6af)
- Kirkpatrick, J. D., Marocco, F., Gelino, C. R., et al. 2024, *ApJS*, 271, 55, doi: [10.3847/1538-4365/ad24e2](https://doi.org/10.3847/1538-4365/ad24e2)
- Konopacky, Q. M., Ghez, A. M., Barman, T. S., et al. 2010, *ApJ*, 711, 1087, doi: [10.1088/0004-637X/711/2/1087](https://doi.org/10.1088/0004-637X/711/2/1087)
- Liebert, J., & Burgasser, A. J. 2007, *ApJ*, 655, 522, doi: [10.1086/509882](https://doi.org/10.1086/509882)
- Liu, M. C., Dupuy, T. J., Bowler, B. P., Leggett, S. K., & Best, W. M. J. 2012, *ApJ*, 758, 57, doi: [10.1088/0004-637X/758/1/57](https://doi.org/10.1088/0004-637X/758/1/57)
- Lodieu, N., Alonso, R., González Hernández, J. I., et al. 2015, *A&A*, 584, A128, doi: [10.1051/0004-6361/201527464](https://doi.org/10.1051/0004-6361/201527464)

- Looper, D. L., Burgasser, A. J., Kirkpatrick, J. D., & Swift, B. J. 2007a, *ApJL*, 669, L97, doi: [10.1086/523812](https://doi.org/10.1086/523812)
- Looper, D. L., Kirkpatrick, J. D., & Burgasser, A. J. 2007b, *AJ*, 134, 1162, doi: [10.1086/520645](https://doi.org/10.1086/520645)
- Looper, D. L., Kirkpatrick, J. D., Cutri, R. M., et al. 2008, *ApJ*, 686, 528, doi: [10.1086/591025](https://doi.org/10.1086/591025)
- Lueber, A., Kitzmann, D., Bowler, B. P., Burgasser, A. J., & Heng, K. 2022, *ApJ*, 930, 136, doi: [10.3847/1538-4357/ac63b9](https://doi.org/10.3847/1538-4357/ac63b9)
- Luhman, K. L., Alves de Oliveira, C., Baraffe, I., et al. 2024, *ApJ*, 975, 162, doi: [10.3847/1538-4357/ad7b19](https://doi.org/10.3847/1538-4357/ad7b19)
- Luhman, K. L., Esplin, T. L., & Loutrel, N. P. 2016, *ApJ*, 827, 52, doi: [10.3847/0004-637X/827/1/52](https://doi.org/10.3847/0004-637X/827/1/52)
- Luhman, K. L., Mamajek, E. E., Allen, P. R., & Cruz, K. L. 2009, *ApJ*, 703, 399, doi: [10.1088/0004-637X/703/1/399](https://doi.org/10.1088/0004-637X/703/1/399)
- Luhman, K. L., Mamajek, E. E., Shukla, S. J., & Loutrel, N. P. 2017, *AJ*, 153, 46, doi: [10.3847/1538-3881/153/1/46](https://doi.org/10.3847/1538-3881/153/1/46)
- Luhman, K. L., & Sheppard, S. S. 2014, *ApJ*, 787, 126, doi: [10.1088/0004-637X/787/2/126](https://doi.org/10.1088/0004-637X/787/2/126)
- Luhman, K. L., Whitney, B. A., Meade, M. R., et al. 2006, *ApJ*, 647, 1180, doi: [10.1086/505572](https://doi.org/10.1086/505572)
- Luhman, K. L., Patten, B. M., Marengo, M., et al. 2007, *ApJ*, 654, 570, doi: [10.1086/509073](https://doi.org/10.1086/509073)
- Luhman, K. L., Loutrel, N. P., McCurdy, N. S., et al. 2012, *ApJ*, 760, 152, doi: [10.1088/0004-637X/760/2/152](https://doi.org/10.1088/0004-637X/760/2/152)
- Mace, G. N., Kirkpatrick, J. D., Cushing, M. C., et al. 2013, *ApJS*, 205, 6, doi: [10.1088/0067-0049/205/1/6](https://doi.org/10.1088/0067-0049/205/1/6)
- Mainzer, A., Cushing, M. C., Skrutskie, M., et al. 2011, *ApJ*, 726, 30, doi: [10.1088/0004-637X/726/1/30](https://doi.org/10.1088/0004-637X/726/1/30)
- Manjavacas, E., Goldman, B., Reffert, S., & Henning, T. 2013, *A&A*, 560, A52, doi: [10.1051/0004-6361/201321720](https://doi.org/10.1051/0004-6361/201321720)
- Martín, E. L., Brandner, W., Bouy, H., et al. 2006, *A&A*, 456, 253, doi: [10.1051/0004-6361:20054186](https://doi.org/10.1051/0004-6361:20054186)
- McElwain, M. W., & Burgasser, A. J. 2006, *AJ*, 132, 2074, doi: [10.1086/508199](https://doi.org/10.1086/508199)
- McKinney, W., et al. 2010, in Proceedings of the 9th Python in Science Conference, Vol. 445, Austin, TX, 51–56
- Metchev, S. A., Kirkpatrick, J. D., Berriman, G. B., & Looper, D. 2008, *ApJ*, 676, 1281, doi: [10.1086/524721](https://doi.org/10.1086/524721)
- Mohandas, A., Smart, R. L., Reylé, C., et al. 2025, arXiv e-prints, arXiv:2503.22559, doi: [10.48550/arXiv.2503.22559](https://doi.org/10.48550/arXiv.2503.22559)
- Morgan, D. P., West, A. A., Garcés, A., et al. 2012, *AJ*, 144, 93, doi: [10.1088/0004-6256/144/4/93](https://doi.org/10.1088/0004-6256/144/4/93)
- Morrissey, S. J., Burgasser, A. J., de Graaff, A., McConachie, L., & Brammer, G. 2025, arXiv e-prints, arXiv:2511.01167, doi: [10.48550/arXiv.2511.01167](https://doi.org/10.48550/arXiv.2511.01167)
- Mosby, G., Rauscher, B. J., Bennett, C., et al. 2020, *Journal of Astronomical Telescopes, Instruments, and Systems*, 6, 046001, doi: [10.1117/1.JATIS.6.4.046001](https://doi.org/10.1117/1.JATIS.6.4.046001)
- Muench, A. A., Lada, C. J., Luhman, K. L., Muzerolle, J., & Young, E. 2007, *AJ*, 134, 411, doi: [10.1086/518560](https://doi.org/10.1086/518560)
- Pecaut, M. J., & Mamajek, E. E. 2013, *ApJS*, 208, 9, doi: [10.1088/0067-0049/208/1/9](https://doi.org/10.1088/0067-0049/208/1/9)
- Pedregosa, F., Varoquaux, G., Gramfort, A., et al. 2011, *Journal of Machine Learning Research*, 12, 2825
- Peterson, W., Birdsall, T., & Fox, W. 1954, *Transactions of the IRE professional group on information theory*, 4, 171
- Radigan, J., Jayawardhana, R., Lafrenière, D., et al. 2013, *ApJ*, 778, 36, doi: [10.1088/0004-637X/778/1/36](https://doi.org/10.1088/0004-637X/778/1/36)
- Radigan, J., Lafrenière, D., Jayawardhana, R., & Artigau, E. 2014, *ApJ*, 793, 75, doi: [10.1088/0004-637X/793/2/75](https://doi.org/10.1088/0004-637X/793/2/75)
- Raymond, S. N., Szkody, P., Hawley, S. L., et al. 2003, *AJ*, 125, 2621, doi: [10.1086/374762](https://doi.org/10.1086/374762)

- Rayner, J. T., Toomey, D. W., Onaka, P. M., et al. 2003, *PASP*, 115, 362
- Rebassa-Mansergas, A., Gänsicke, B. T., Schreiber, M. R., Koester, D., & Rodríguez-Gil, P. 2010, *MNRAS*, 402, 620, doi: [10.1111/j.1365-2966.2009.15915.x](https://doi.org/10.1111/j.1365-2966.2009.15915.x)
- Reid, I. N., Lewitus, E., Allen, P. R., Cruz, K. L., & Burgasser, A. J. 2006a, *AJ*, 132, 891, doi: [10.1086/505626](https://doi.org/10.1086/505626)
- Reid, I. N., Lewitus, E., Burgasser, A. J., & Cruz, K. L. 2006b, *ApJ*, 639, 1114, doi: [10.1086/499484](https://doi.org/10.1086/499484)
- Robert, J., Gagné, J., Artigau, É., et al. 2016, *ApJ*, 830, 144, doi: [10.3847/0004-637X/830/2/144](https://doi.org/10.3847/0004-637X/830/2/144)
- Sahlmann, J., Lazorenko, P. F., Ségransan, D., et al. 2014, *A&A*, 565, A20, doi: [10.1051/0004-6361/201323208](https://doi.org/10.1051/0004-6361/201323208)
- Sahlmann, J., Burgasser, A. J., Martín, E. L., et al. 2015, *A&A*, 579, A61, doi: [10.1051/0004-6361/201425536](https://doi.org/10.1051/0004-6361/201425536)
- Sahlmann, J., Burgasser, A. J., Bardalez Gagliuffi, D. C., et al. 2020, *MNRAS*, 495, 1136, doi: [10.1093/mnras/staa1235](https://doi.org/10.1093/mnras/staa1235)
- Sahlmann, J., Dupuy, T. J., Burgasser, A. J., et al. 2021, *MNRAS*, 500, 5453, doi: [10.1093/mnras/staa3577](https://doi.org/10.1093/mnras/staa3577)
- Schmidt, S. J., West, A. A., Burgasser, A. J., Bochanski, J. J., & Hawley, S. L. 2010, *AJ*, 139, 1045, doi: [10.1088/0004-6256/139/3/1045](https://doi.org/10.1088/0004-6256/139/3/1045)
- Schneider, A. C., Cushing, M. C., Kirkpatrick, J. D., et al. 2014, *AJ*, 147, 34, doi: [10.1088/0004-6256/147/2/34](https://doi.org/10.1088/0004-6256/147/2/34)
- Schneider, A. C., Greco, J., Cushing, M. C., et al. 2016a, *ApJ*, 817, 112, doi: [10.3847/0004-637X/817/2/112](https://doi.org/10.3847/0004-637X/817/2/112)
- Schneider, A. C., Windsor, J., Cushing, M. C., Kirkpatrick, J. D., & Shkolnik, E. L. 2017, *AJ*, 153, 196, doi: [10.3847/1538-3881/aa6624](https://doi.org/10.3847/1538-3881/aa6624)
- Schneider, A. C., Windsor, J., Cushing, M. C., Kirkpatrick, J. D., & Wright, E. L. 2016b, *ApJL*, 822, L1, doi: [10.3847/2041-8205/822/1/L1](https://doi.org/10.3847/2041-8205/822/1/L1)
- Sheppard, S. S., & Cushing, M. C. 2009, *AJ*, 137, 304, doi: [10.1088/0004-6256/137/1/304](https://doi.org/10.1088/0004-6256/137/1/304)
- Siegler, N., Close, L. M., Burgasser, A. J., et al. 2007, *AJ*, 133, 2320, doi: [10.1086/513273](https://doi.org/10.1086/513273)
- Stassun, K. G., Mathieu, R. D., & Valenti, J. A. 2006, *Nature*, 440, 311, doi: [10.1038/nature04570](https://doi.org/10.1038/nature04570)
- Thompson, M. A., Kirkpatrick, J. D., Mace, G. N., et al. 2013, *PASP*, 125, 809, doi: [10.1086/671426](https://doi.org/10.1086/671426)
- Triaud, A. H. M. J., Burgasser, A. J., Burdanov, A., et al. 2020, *Nature Astronomy*, 4, 650, doi: [10.1038/s41550-020-1018-2](https://doi.org/10.1038/s41550-020-1018-2)
- Tu, Z., Wang, S., Chen, X., & Liu, J. 2025, arXiv e-prints, arXiv:2510.02026, doi: [10.48550/arXiv.2510.02026](https://doi.org/10.48550/arXiv.2510.02026)
- Žerjal, M., Dominguez-Tagle, C., Sedighi, N., et al. 2025, arXiv e-prints, arXiv:2503.22497, doi: [10.48550/arXiv.2503.22497](https://doi.org/10.48550/arXiv.2503.22497)
- Zhou, T., Theissen, C. A., Burgasser, A. J., Best, W. M. J., & Feeder, S. J. 2024, *Research Notes of the American Astronomical Society*, 8, 102, doi: [10.3847/2515-5172/ad3f16](https://doi.org/10.3847/2515-5172/ad3f16)